Numerical Solution to the Time-Dependent Maxwell Equations in Two-Dimensional Singular Domains: The Singular Complement Method

F. Assous,* P. Ciarlet, Jr.,† and J. Segré*

*CEA/DAM–DIF, BP12-91680, Bruyères-le-Châtel, France; and †UMA, ENSTA,
32 boulevard Victor, 75739 Paris Cedex 15, France
E-mail: assous@bruyeres.cea.fr

In this paper, we present a method to solve numerically the time-dependent Maxwell equations in nonsmooth and nonconvex domains. Indeed, the solution is not of regularity H^1 (in space) in general. Moreover, the space of H^1-regular fields is not dense in the space of solutions. Thus an H^1-conforming Finite Element Method can fail, even with mesh refinement. The situation is different than in the case of the Laplace problem or of the Lamé system, for which mesh refinement or the addition of conforming singular functions work. To cope with this difficulty, the Singular Complement Method is introduced. This method consists of adding some well-chosen test functions. These functions are derived from the singular solutions of the Laplace problem. Also, the SCM preserves the interesting features of the original method: easiness of implementation, low memory requirements, small cost in terms of the CPU time. To ascertain its validity, some concrete problems are solved numerically.   © 2000 Academic Press

Key Words: Maxwell's equation; singularities; reentrant corners; conforming finite elements.

1. INTRODUCTION

In recent years, modeling and solving numerically problems which couple charged particles to electromagnetic fields has given rise to challenging mathematical and scientific computing developments. In the industry, a variety of examples can be thought of, such as the ion or electron injectors for particle accelerators, the free electron lasers, or the hyperfrequency devices. The mathematical model which is most relevant in describing the physics of these devices is the time-dependent coupled Vlasov–Maxwell system of equations.

In this context, and *independently* of any geometrical considerations, we have developed a method to solve the time-dependent Maxwell equations (see [6]), which has been designed with the help of H(curl) $\cap$ H(div)-conforming Finite Elements.[1] In this method, the computed electromagnetic field is continuous (this condition is recommended to reduce the noise of the solution of the *coupled problem* [7]), and the numerical scheme does not require solving a linear system at each time step. The conditions on the divergence of the fields are treated as constraints and dualized as such by using Lagrange multipliers, which yields a saddle-point formulation. We refer the reader to [6] for an in-depth analysis of the method and for a detailed bibliography. This method is also interesting as nodal finite elements (Lagrange P^1) are used, the implementation of which is common and easy.

However, a number of industrial structures and objects that must be modeled present a surface with edges, corners, etc., be it intentionally or not. The existence of those geometrical distinctive features—of those *geometrical singularities*—on the boundaries of the domains which must be studied can create singular fields, that is unbounded fields (in the neighborhood of those singularities). Moreover, this difficulty is not restricted to exterior problems, as it must be dealt with in bounded domains too, as soon as the boundary of the domain contains such singularities. Such is the case in the following situations:

• The geometrical singularities are an active part of the device, for instance to generate the powerful electromagnetic fields which are required to extract a strong electron current at a velvet cathode in a microwave generator.

• The geometrical singularities are only the consequence of constraints on the *a priori* configuration of the device, and it is mandatory to be able to control the induced negative effects, such as the above-mentioned powerful fields which can produce breakdowns.

Finally, let us note that the presence of singularities changes the solution in *the whole domain* and not only in their neighborhood. In this respect, they have a *nonlocal* effect. We present an example which illustrates the effect of singularities in a numerical computation. Here, we focus on the *qualitative* aspect of the results only.

We consider the propagation of a wave in a stub filter (see Fig. 1), which is propagated or evanescent, depending on both the frequency of the wave and on the size of the stubs. For given frequencies, the guide is transversally closed, thus becoming a plain waveguide of rectangular section. In the example below, the guide is illuminated by a wave, the time-signal of which is included in the range of the frequencies of propagated modes.

This filtering phenomenon can be modeled by the *time-dependent* Maxwell equations. The result of a simulation for a two-stub filter is shown in the left-hand side of Fig. 1 for an incident wave with the frequency of a propagated mode. The data and the geometry are assumed to be independent of one of the space variables, and therefore the model is 2D. Contrary to the physics, the result is that of an evanescent mode for this frequency. In order to emphasize the connection between the odd filtering effect and the reentrant corners (the singularities), these edges are smoothed; that is, they are replaced by smooth structures with a radius in the order of 1/20th of the wavelength. The results that are obtained in this case (see Fig. 1 (right)) confirm that there is indeed a propagated mode. However, the "smoothing" of the corners yields two problems which must be addressed:

---

[1] Thanks to recent results [16], choosing a piecewise smooth H(curl) $\cap$ H(div)-conforming FE amounts to using an H^1-conforming FE.
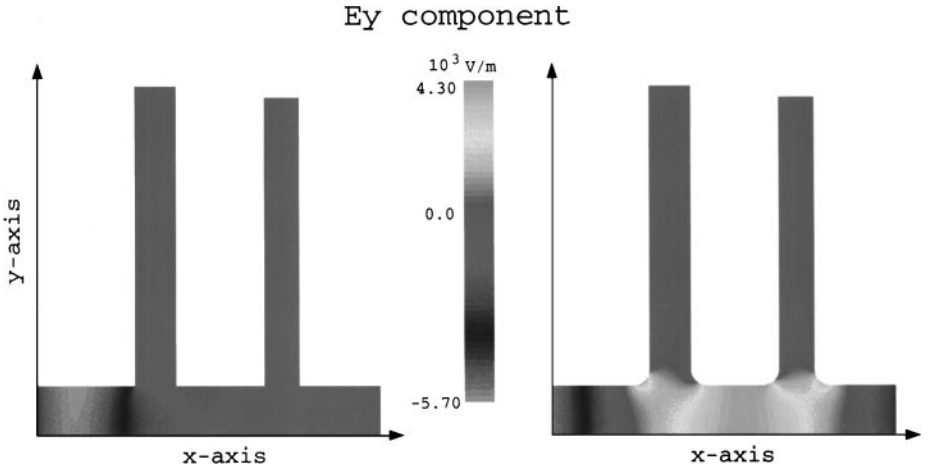
FIG. 1. E_y component—sharp corners: evanescent mode in the guide—smoothed corners: propagated mode in the guide.

• it requires a mesh refinement in the neighborhood of the reentrant corners (here, by a factor of 10), which leads to high computational costs.

• The original geometry of the device is modified, and the simulation thus loses its accuracy. Moreover, by smoothing the singularites, the very strong fields are numerically underestimated, whereas one of the goals of the simulation is to control the negative effects (breakdowns, etc.) by estimating them precisely.

Let us note however that there is no problem (in this configuration) as far as the B_z magnetic induction is concerned, either for the original geometry or for the smoothed geometry (cf. Fig. 2). In this respect, B_z is sufficiently *smooth*.

In order to address the problems raised by the singularities, we provided a mathematical analysis of the singularities of Maxwell's equations in a nonconvex geometry [5]. The key point is the following: in a nonconvex polygonal (or polyhedral in 3D) domain Ω, the
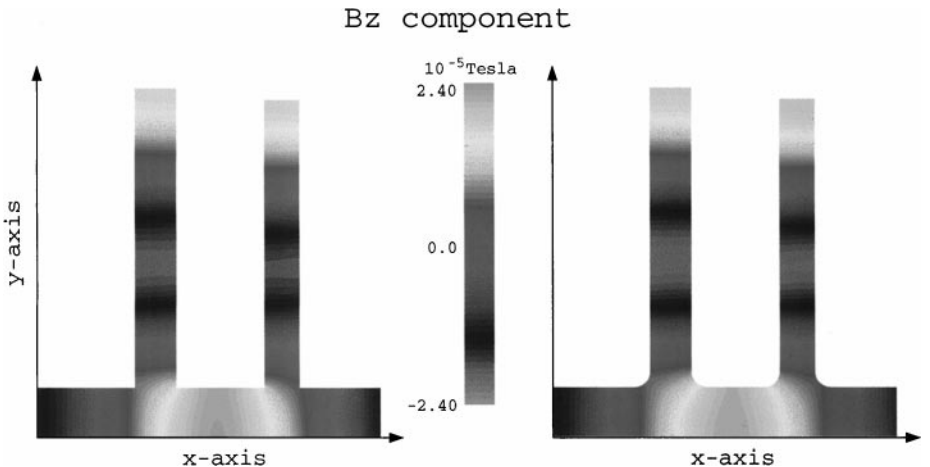

FIG. 2. Smooth B_z component, the mode is propagated in both cases.

solutions (electric field and magnetic induction) of Maxwell's equations at a given time t do not belong to $H^1(\Omega)^2$ (or $H^1(\Omega)^3$) as is the case in a convex domain, but only to $H(\text{curl}, \Omega) \cap H(\text{div}, \Omega)$. In other words, the "physical" solution of Maxwell's equations, which only belongs to the functional space $H(\text{curl}, \Omega) \cap H(\text{div}, \Omega)$, goes to infinity when one comes close to a reentrant edge or a reentrant corner. It does not coincide with the "smoothed" solution, that is, the one computed thanks to a formulation of the problem in $H^1(\Omega)^2$. In addition, there is no hope to converge to the "physical" solution by using mesh refinement, as the space of fields which belongs to $H^1(\Omega)^2$ is *not dense* in the space of fields which belongs to $H(\text{curl}, \Omega) \cap H(\text{div}, \Omega)$ (this situation also occurs in 3D). This is major difficulty as far as the numerical computation of solutions is concerned.

Note that the numerical methods based on edge finite elements which are conforming in $H(\text{curl}, \Omega)$ [21], or those based on finite volumes on orthogonal meshes (in the 2D case) [18], allow one to approximate the solution. Indeed, the degrees of freedom of these methods are located on the edges of the mesh, and therefore they do not "carry" the geometrical singularities. Nevertheless, in order to get a precise knowledge of the solution close to the singularities, one must perform very significant mesh refinements (which makes them hard to use in some situations). What is more, in our case, using Nédélec's second family of nodal finite elements [22], which are also conforming in $H(\text{curl}, \Omega)$, can be problematic. As a matter of fact, the regularity required to define the associated moments (cf. [9]) is not automatically fulfilled by the solution of the time-dependent Maxwell equations.

Still, for most applications, computing the behavior of the solution outside of a neighborhood of the singularity is not sufficient. It is required that one computes the solution precisely as close to this singularity as is possible.

In order to achieve sufficient precision, one can *a priori* try to use singular functions methods. These methods, which have been developed for elliptic problems (see the earlier works in [12]), consist of augmenting the basis of numerical functions by adding a singular function (H^1-*conforming* at the reentrant corner). They are widely used when the lack of regularity of the solution leads to a slow convergence of the nodal finite element method. In this case, a carefully chosen *refinement* of the mesh would have been sufficient, and the singular function method can be viewed as an alternative. Here, the key point is that the numerical basis, with or without the addition of singular functions or mesh refinement, already spans the whole set of solutions when the mesh size goes to zero.

Unfortunately, this method *cannot* be applied to solving Maxwell's equations in a singular domain, as the solution computed by a nodal finite element method does not span the whole space of the physical solutions (cf. the density problem mentioned above). Once again, it is not a matter of speed of convergence, and a mesh refinement or the addition of a singular function does not improve the overall numerical method.

To cope with this difficulty, we have developed a new method for solving time-dependent Maxwell equations in singular domains, called the *Singular Complement Method (SCM)*. One of its advantages is that it can easily be included in already existing numerical codes, which allows one to increase their domain of application. As a matter of fact, it makes them usable in the presence of geometrical singularities simply by adding a small number of functionalities, without having to rewrite them in their entirety.

The SCM is based on an orthogonal decomposition of the solution into a regular part and a singular part. The original ideas can be found in the works of Grisvard (see [14], [15] and the references herein). Let us consider the Laplace equation with a right-hand side in $L^2(\Omega)$. Its solution belongs to $H^2(\Omega)$ when the domain is smooth (or convex), but it only

belongs to $H^{1+s}(\Omega)$, with $1/2 < s < 1$, when there are geometrical singularities (see [15] for a 2D domain, and also [10], [14] for a 3D domain). Relying on an *ad hoc* decomposition of $L^2(\Omega)$, Grisvard showed that it is possible to split the solution in a regular (in $H^2(\Omega)$) part and a singular part. Along the same lines, let us mention another approach developed by Hazard *et al.* (see [8], [17]) for the treatment of the time-harmonic Maxwell equations, which is also based on a decomposition of the space of solutions. Their decomposition is however slightly different from ours, thus leading to a different numerical scheme.

We introduced an orthogonal decomposition of the solution of Maxwell's equations, which is mathematically analyzed in [5]. We recall the principles of the method in Section 2. Hereafter, we build a constructive method for solving the original problem, and its associated numerical algorithm, which are detailed in Sections 3 and 4. The algorithm makes use of the explicit knowledge of the expression of the singularities near the reentrant corners. In Section 5, we present some numerical results which illustrate the efficiency of the SCM, applied to a number of realistic devices.

2. A MATHEMATICAL ANALYSIS OF THE PROBLEM

2.1. Maxwell's Equations

Let us consider a bounded, connected, and simply connected open subset Ω of $\mathbb{R}^2$, the boundary of which is called Γ; let the infinite cylinder $\Omega \times \mathbb{R}$ be the physical domain. Let $\nu = (\nu_x, \nu_y, 0)^T$ be the outward unit normal to the domain, with the exception of the infinite edges. If we let c and ε_0 be, respectively, the speed of light and the dielectric permittivity, Maxwell's equations read

$$\frac{\partial \mathcal{E}}{\partial t} - c^2 \, \mathbf{curl} \, \mathcal{B} = -\frac{1}{\varepsilon_0} \mathcal{J}, \tag{1}$$

$$\frac{\partial \mathcal{B}}{\partial t} + \mathbf{curl} \, \mathcal{E} = 0, \tag{2}$$

$$\mathrm{div} \, \mathcal{E} = \frac{\rho}{\varepsilon_0}, \tag{3}$$

$$\mathrm{div} \, \mathcal{B} = 0, \tag{4}$$

where $\mathcal{E}$ is the electric field, $\mathcal{B}$ is the magnetic induction, and ρ and $\mathcal{J}$ are the charge and current densities. These quantities depend on the space variable $\mathbf{x}$ and on the time variable t. Note that the above system of equations (1–4) is considered inside $\Omega \times \mathbb{R}$.

These equations are supplied with appropriate bounday conditions. In order to simplify the presentation, let us assume first that the boundary is a perfect conductor. In Section 4, the extension to the Silver–Müller boundary condition will be handled: it can model either an absorbing medium outside of the domain or an incident wave. For the moment, let us take the conditions

$$\mathcal{E} \times \nu = 0 \text{ on } \Gamma \times \mathbb{R}, \tag{5}$$

$$\mathcal{B} \cdot \nu = 0 \text{ on } \Gamma \times \mathbb{R}. \tag{6}$$

The charge conservation equation is a consequence of equations (1–3) and reads

$$\frac{\partial \rho}{\partial t} + \mathrm{div} \, \mathcal{J} = 0. \tag{7}$$

Last, initial conditions are provided (for instance at time $t = 0$)

$$\mathcal{E}(\cdot, 0) = \mathcal{E}_0, \tag{8}$$

$$\mathcal{B}(\cdot, 0) = \mathcal{B}_0, \tag{9}$$

where the couple $(\mathcal{E}_0, \mathcal{B}_0)$ depends only on the variable $\mathbf{x}$.

In what follows, it is assumed that both the data and the initial conditions *do not depend* on the transverse variable z. Then the original problem can be identified with a problem the domain of which is a section of the infinite cylinder, that is Ω. As a matter of fact, the set of first order in time equations (1–4) can be rewritten equivalently as two decoupled sets of first order in time equations. If, for the field $\mathcal{Z} = (Z_x, Z_y, Z_z)^T$ of $\mathbb{R}^3$ one uses the notation $\mathbf{Z} = (Z_x, Z_y)^T$, the first set of equations is of unknowns $(\mathbf{E}, B_z)$, i.e., the so-called TE mode, with data $\mathbf{J}$ and ρ, while the second set is of unknowns $(E_z, \mathbf{B})$ with datum J_z (the TM mode).

In the 2D case, let us note that there exists a scalar curl operator, denoted by curl, and a vector curl operator, denoted by **curl**. Both systems can be equivalently formulated as second order in time systems (see [6]). The TE mode can be written as

$$\frac{\partial^2 \mathbf{E}}{\partial t^2} + c^2 \, \mathbf{curl} \, \mathrm{curl} \, \mathbf{E} = -\frac{1}{\varepsilon_0} \frac{\partial \mathbf{J}}{\partial t}, \tag{10}$$

$$\mathrm{div} \, \mathbf{E} = \frac{\rho}{\varepsilon_0}, \tag{11}$$

$$\frac{\partial^2 B_z}{\partial t^2} - c^2 \Delta B_z = \frac{1}{\varepsilon_0} \, \mathrm{curl} \, \mathbf{J}. \tag{12}$$

Let $\tau = (\nu_y, -\nu_x)^T$ be the tangential vector associated to the normal vector $\nu = (\nu_x, \nu_y)^T$. With these notations, the perfectly conducting boundary condition can be written, for the electric field

$$\mathbf{E} \cdot \tau = 0, \tag{13}$$

and for the magnetic induction

$$\frac{\partial B_z}{\partial \nu} - \frac{1}{c^2 \varepsilon_0} \mathbf{J} \cdot \tau = 0. \tag{14}$$

In addition to these conditions, the second order in time system of equations is closed with the help of initial conditions on $\partial \mathbf{E}/\partial t$ and $\partial B_z/\partial t$

$$\frac{\partial \mathbf{E}}{\partial t}(\cdot, 0) = c^2 \, \mathbf{curl} \, B_{z0} - \frac{1}{\varepsilon_0} \mathbf{J}(\cdot, 0), \tag{15}$$

$$\frac{\partial B_z}{\partial t}(\cdot, 0) = -\mathrm{curl} \, \mathbf{E}_0. \tag{16}$$

The TM system could be written in the same way. In this paper, we focus on the above system, keeping in mind that one can also handle the other system with no additional difficulty (see [5] for more details). Also, we assume in the following that the domain Ω has a single reentrant corner. We refer the reader to [5] for the more general case, that is

a polygon with several reentrant corners. Again, there is no additional difficulty, with the exception of the formulas, which become a little bit more complicated.

The scalar product of $L^2(\Omega)$ is denoted by $(f \mid g)_0 = \int_\Omega fg \, d\mathbf{x}$ and the related norm is $\| \cdot \|_0$. Let us introduce the functional spaces

$$L_0^2(\Omega) = \{f \in L^2(\Omega), (f \mid 1)_0 = 0\}, \tag{17}$$

$$H_0(\text{curl}, \Omega) = \{\mathbf{u} \in H(\text{curl}, \Omega), \mathbf{u} \cdot \tau = 0 \text{ on } \Gamma\}, \tag{18}$$

$$V = \{\mathbf{u} \in H_0(\text{curl}, \Omega), \text{div } \mathbf{u} = 0\}; \tag{19}$$

V is equipped with the canonical scalar product of H (curl, Ω):

$$(\mathbf{u}, \mathbf{v}) \mapsto (\mathbf{u} \mid \mathbf{v})_{0,\text{curl}} \overset{\text{def}}{=} (\mathbf{u} \mid \mathbf{v})_0 + (\text{curl } \mathbf{u} \mid \text{curl } \mathbf{v})_0.$$

In the present case, or more generally in a nonconvex domain with several reentrant corners, the space V is not included in $H^1(\Omega)^2$ any more (see [14] for instance). It is thus natural to introduce the regularized space V_R of V:

$$V_R = \{\mathbf{u} \in H^1(\Omega)^2, \text{div } \mathbf{u} = 0, \mathbf{u} \cdot \tau = 0 \text{ on } \Gamma\} = V \cap H^1(\Omega)^2. \tag{20}$$

It is proved in [1] (see also the Introduction) that the B_z component, as the solution of a wave equation, always belongs to $H^1(\Omega)$, even in a nonconvex domain. It can therefore be computed numerically without any problem. On the contrary, the electric field $\mathbf{E}$, which is the solution of Maxwell's equation (10), (11), does not belong to $H^1(\Omega)^2$ as would be the case in a convex domain, but it only belongs to V. This is the reason why we consider only the computation of the field $\mathbf{E}$ in what follows.

Let us introduce the time-dependent problem:

Given a current $\mathbf{J}(t)$ *such that* div $\mathbf{J} = 0$, *and two initial data* $\mathbf{E}_0$ *and* $\mathbf{E}_1$, *find* $\mathbf{E}(t) \in H(\text{curl}, \Omega)$ *such that*

$$\frac{\partial^2 \mathbf{E}}{\partial t^2} + c^2 \, \textbf{curl} \text{ curl } \mathbf{E} = -\frac{1}{\varepsilon_0} \frac{\partial \mathbf{J}}{\partial t}, \tag{21}$$

$$\text{div } \mathbf{E} = 0, \tag{22}$$

$$\mathbf{E} \cdot \tau = 0 \text{ on } \Gamma, \tag{23}$$

with the classical initial conditions $\mathbf{E}(0) = \mathbf{E}_0$ and $\partial \mathbf{E}/\partial t(0) = \mathbf{E}_1$. It can be written in a variational form:

Find $\mathbf{E}(t) \in H_0(\text{curl}, \Omega)$ *such that*

$$\frac{d^2}{dt^2}(\mathbf{E} \mid \mathbf{F})_0 + c^2(\text{curl } \mathbf{E} \mid \text{curl } \mathbf{F})_0 = -\frac{1}{\varepsilon_0} \left(\frac{\partial \mathbf{J}}{\partial t} \, \middle| \, \mathbf{F} \right)_0 \quad \forall \mathbf{F} \in H_0(\text{curl}, \Omega), \tag{24}$$

$$\text{div } \mathbf{E} = 0, \tag{25}$$

with the same initial conditions. One could also formulate the equivalent of (21)–(23) and of (24), (25) in $H_0(\text{curl}, \Omega) \cap H(\text{div}, \Omega)$ or in V.

Thanks to [20], these exists one and only one solution to these problems.

Remark 2.1. The problem (21)–(23) is written in the absence of charges, that is with div $\mathbf{E} = 0$. One can consider the problem with charges, where (22) is replaced, for $\rho \in L^2(\Omega)$, by div $\mathbf{E} = \rho/\varepsilon_0$, and where div $\mathbf{J} = 0$ is replaced by $\partial\rho/\partial t + \text{div } \mathbf{J} = 0$. As a matter of fact, it can still be reduced to the divergence-free problem. In order to do so, one can, for instance, let $\mathbf{E}^\star = \mathbf{E} - \nabla\psi$, with ψ the unique element of $H_0^1(\Omega)$ that satisfies $\Delta\psi = \rho/\varepsilon_0$; this equation can be solved using its usual variational counterpart. This method is often called the Poisson correction (see, among others, [7] and [18] for numerical experiments). In the present case, ρ is a time-dependent function, and it is best to avoid the solution to a linear system at each time step. To address this difficulty, we have built a method which is a generalization of the method we apply in this paper, that is, the decomposition of the solution in a regular part and a singular part in V, to the case of fields with a nonvanishing divergence (see [2]).

2.2. A Decomposition of the Solution in Regular and Singular Parts

Let us briefly recall, without proof, some useful theoretical results in order to understand better the construction of the numerical method. The reader is referred to [5] for a thorough study.

The underlying principle of the method consists of relating the singular solutions of Maxwell's equations to those of the Laplace problem, the properties of the latter having been investigated in a detailed manner (cf. [10, 14, 15]). On the one hand, there is the orthogonal decomposition of $L_0^2(\Omega)$

$$L_0^2(\Omega) = \Delta(\Phi_R) \overset{\perp}{\oplus} S_N, \tag{26}$$

where $\Delta(\Phi_R)$ is the range of Φ_R by the operator Δ, with

$$\Phi_R = \left\{ \phi \in H^2(\Omega)/\mathbb{R}, \left. \frac{\partial\phi}{\partial v} \right|_\Gamma = 0 \right\},$$

and S_N is characterized as the set of distributions $\psi \in L_0^2(\Omega)$ such that

$$\Delta\psi = 0 \text{ in } \mathcal{D}'(\Omega), \tag{27}$$

$$\frac{\partial\psi}{\partial v} = 0 \text{ on } \Gamma. \tag{28}$$

Thanks to Grisvard [15], S_N is a finite dimensional vector space, it dimension being equal to the number of reentrant corners, that is 1 in our case. Let us call p_S its basis.

On the other hand, we proved the following result:

LEMMA 2.1. *The scalar operator* curl *is an isomorphism from V onto* $L_0^2(\Omega)$. *In addition, the* L^2*-norm of the curl defines on V a norm, which is equivalent to the norm* $\|\cdot\|_{0,\text{curl}}$.

Let V be equipped with the scalar product induced by $\mathbf{v} \mapsto \|\text{curl } \mathbf{v}\|_0$. In this case, the isomorphism of Lemma 2.1 preserves orthogonality. Having proved that the space V_R, as well as its range by the scalar curl operator, are closed in V and $L_0^2(\Omega)$, respectively, it is valid to introduce their orthogonal supplementary subspaces. This allows one to conclude that the orthogonal of curl V_R in $L_0^2(\Omega)$, denoted by $(\text{curl } V_R)^\perp$, is equal to S_N. In this way, one obtains a result concerning the orthogonal decomposition of vector fields in V:

THEOREM 2.1. *The space V can be split in the orthogonal sum $V = V_R \overset{\perp}{\oplus} V_S$, where V_S is a vector space of dimension 1, defined by* curl $V_S = S_N$.

The electric field, solution of (21)–(23), depends continuously on the time variable with values in V [1]. Then, at any time t, one obtains the (orthogonal) decomposition

$$\mathbf{E}(t) = \mathbf{E}_R(t) + \mathbf{E}_S(t). \tag{29}$$

The field $\mathbf{E}_R \in V_R$ is called the regular part of the solution, whereas the field $\mathbf{E}_S \in V_S$ is called the singular part. Moreover, the space V_S is of dimension 1, so one may write

$$\mathbf{E}(t) = \mathbf{E}_R(t) + \kappa(t)\mathbf{v}_S, \tag{30}$$

with $\mathbf{v}_S$ a basis of V_S and κ a function which is smooth in time (at least continuous, cf. [1]).

Remark 2.2. 1. In the particular cases when $\mathbf{E}_S = 0$ (i.e., the domain is convex), or when the singular coefficient κ is zero, one has obviously $\mathbf{E} = \mathbf{E}_R \in H^1(\Omega)^2$. This property must be preserved numerically: this fact is illustrated in Section 5.

2. When the domain Ω has K reentrant corners, $\dim(V_S) = K$. Then, for $(\mathbf{v}_S^j)_{1 \leq j \leq K}$ a basis of V_S

$$\mathbf{E}(t) = \mathbf{E}_R(t) + \sum_{1 \leq j \leq K} \kappa_j(t)\mathbf{v}_S^j, \tag{31}$$

where $(\kappa_j)_{1 \leq j \leq K}$ are K smooth functions (cf. [1]).

3. A NUMERICAL METHOD TO COMPUTE THE SOLUTION

Starting from the orthogonal decomposition obtained previously, it is possible to build a method, which allows one to compute numerically the solution.

Remark 3.1. Let us stress the fact that this method can be easily included into already existing codes, without the costly procedure of rewriting them entirely. Here, we are simply stating that a code which computes the solution of Maxwell's equations in convex domains actually computes the regular part, as the singular part is always equal to zero in this case. Thus, the method we present here provides an extension of the range of the code to the case of nonconvex (and nonsmooth) domains.

It can be summarized in two steps:

1. *Determination of a basis of V_S.* One must solve a static problem. The computations are carried out only once as an initialization procedure.

2. *Solution to the time-dependent problem* (24), (25). It will then be enough to couple the classical method, which is already available, to the solution of an additional equation, of unknown $\kappa(t)$.

Those steps are enumerated in the following subsections.

3.1. Determination of $\mathbf{v}_S$, a Basis of V_S

3.1.1. *Principle of the Method*

To compute $\mathbf{v}_S$, the isomophism of Lemma 2.1 is used. The framework of the algorithm is as follows:

- **First step**

The space S_N is of dimension 1: one computes first a basis of S_N, that is an nonvanishing element p_S of $L_0^2(\Omega)$, which satisfies to

$$\Delta p_S = 0 \text{ in } \Omega, \tag{32}$$

$$\frac{\partial p_S}{\partial \nu} = 0 \text{ on } \Gamma. \tag{33}$$

- **Second step**

One must then to look for $\mathbf{v}_S \in H(\text{curl}, \Omega)$, the solution of

$$\text{curl } \mathbf{v}_S = p_S \text{ in } \Omega, \tag{34}$$

$$\text{div } \mathbf{v}_S = 0 \text{ in } \Omega, \tag{35}$$

$$\mathbf{v}_S \cdot \tau = 0 \text{ on } \Gamma. \tag{36}$$

Instead of using the direct solution to (34)–(36), it is more practical to make use of another isomorphism (see [5]), which is analogous to the one of Lemma 2.1. It shows that, to $\mathbf{v}_S \in V$, there corresponds one and only one potential $\phi_S \in H^1(\Omega)/\mathbb{R}$ such that

$$-\Delta \phi_S = p_S \text{ in } \Omega, \tag{37}$$

$$\frac{\partial \phi_S}{\partial \nu} = 0 \text{ on } \Gamma. \tag{38}$$

Now, as ϕ_S is sufficiently smooth (i.e., with regularity H^1), one can easily solve this problem with the help of a variational formulation. The computation of $\mathbf{v}_S \in V_S$ then stems from the identity $\mathbf{v}_S = \mathbf{curl}\, \phi_S$.

3.1.2. A Numerical Solution Obtained by Substructuring

Thanks to the above results relating the singular field $\mathbf{v}_S$ to p_S, it is possible to derive some useful information about the expression of the singularities in the neighborhood of the reentrant corner (recall that its counterpart is well known for p_S). In order to benefit from this explicit knowledge, the computational algorithm is built using a substructuring approach.

Let us begin with the computation of p_S. It can be viewed as a generalization of the method originally developed for the Laplace problem by Givoli and Keller [13, 19], their transmission operator being a particular instance of the capacitance operators (see for instance [11]). With this approach, one gets an explicit expression of p_S in a neighborhood of the reentrant corner. Outside of this neighborhood, p_S is smooth, and it can therefore be computed with the help of a classical variational formulation. It should be noted that the information corresponding to the "exact" knowledge of p_S close to the reentrant corner allows one to preserve (numerically) the orthogonality between the regular and singular parts of the solution. This is not the case anymore if one chooses to regularize p_S "locally," by substracting to it its most singular part, that is, this most singular part multiplied by a smooth cut-off function (cf. [15]).

Let us take the domain Ω such as it is pictured on Fig. 3. Its reentrant corner is locally made up of two segments, which intersect at the corner with an angle π/α, $1/2 < \alpha < 1$.
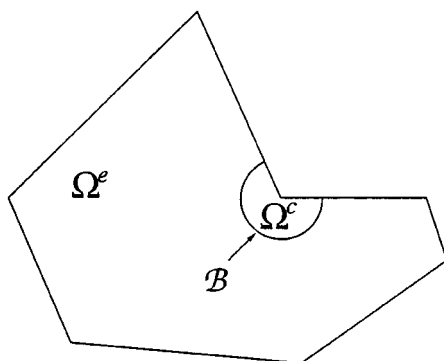
FIG. 3. Shape of the domain Ω.

A partition of Ω in Ω^c and Ω^e is introduced, where Ω^c stands for an open angular sector of radius R centered at the reentrant corner, and where Ω^e is the open domain such that $\Omega^c \cap \Omega^e = \emptyset$ and $\bar{\Omega}^c \cup \bar{\Omega}^e = \bar{\Omega}$. Last, let Γ^c (respectively, Γ^e) denote the boundary of Ω^c (respectively, Ω^e), which is split in $\mathcal{B} \cup \tilde{\Gamma}^c$ (respectively, $\mathcal{B} \cup \tilde{\Gamma}^e$), with $\mathcal{B} = \Gamma^c \cap \Gamma^e$.

In this paper, either a (superscript) ^{c} or ^{e} is added to refer to the restriction of quantities to Ω^c or Ω^e.

First Step: Computation of p_S.

Let us consider the detailed computation of p_S, which is a nonvanishing element of S_N. It can be further divided into four substeps. The first two are "formal" (but still mathematically justified); the other two allow one to compute p_S numerically. Substeps 1 and 2, respectively, consist in finding an expression of p_S^c as a series, then in determining a formula which allows one to recover the coefficient of the series as a function of $p_{S|\mathcal{B}}^c$, and finally in computing a transmission operator on the interface $\mathcal{B}$. After these substeps have been completed, one can pose the problem in Ω^e, the solution of which is p_S^e: it is then computed in Substep 3. From that point on, in Substep 4, one computes the coefficients of the series, using $p_{S|\mathcal{B}}^c = p_{S|\mathcal{B}}^e$, to obtain p_S^c.

1. An expression of the restriction p_S^c:

   Using the separation of variables, one can find analytically the solution in a neighborhood of the reentrant corner. One gets, using the polar coordinates (centered at the corner) $r \leq R, 0 \leq \theta \leq \frac{\pi}{\alpha}$,

   $$p_S^c(r, \theta) = \sum_{n \geq -1} A_n r^{n\alpha} \cos(n\alpha\theta), \qquad \text{with } A_{-1} \neq 0. \tag{39}$$

   Every A_n can be written as an integral of $p_{S|\mathcal{B}}^c$. Let us recall here the expression of the coefficients A_n

   $$A_0 = \frac{\alpha}{\pi} \int_0^{\pi/\alpha} p_S^c(R, \theta)\, d\theta, \tag{40}$$

   $$A_1 = \frac{2\alpha}{\pi} R^{-\alpha} \int_0^{\pi/\alpha} p_S^c(R, \theta) \cos(\alpha\theta)\, d\theta - R^{-2\alpha} A_{-1}, \tag{41}$$

$$A_n = \frac{2\alpha}{\pi} R^{-n\alpha} \int_0^{\pi/\alpha} p_S^c(R, \theta) \cos(n\alpha\theta) \, d\theta, \, \forall n \geq 2, \tag{42}$$

where A_1 is given as a function of A_{-1}, which, by definition, is not equal to zero.

2. The capacitance operator T:

Let ν^c denote the unit outward normal to Ω^c. Thanks to (40)–(42), one can define the capacitance operator $T: p_{S|B}^c \mapsto \frac{\partial p_S^c}{\partial \nu^c}|_B$, by

$$T(p_S^c) = \frac{2\alpha^2}{\pi R} \sum_{n \geq 1} n \left\{ \int_0^{\pi/\alpha} p_S^c(R, \theta') \cos(n\alpha\theta') \, d\theta' \right\} \cos(n\alpha\theta) - 2\alpha \frac{A_{-1}}{R^{\alpha+1}} \cos(\alpha\theta). \tag{43}$$

If we let T_1 stand for the first term of the right-hand side, then

$$T(p_S^c) = T_1(p_S^c) - 2\alpha \frac{A_{-1}}{R^{\alpha+1}} \cos(\alpha\theta). \tag{44}$$

3. Computing the solution p_S^e to the exterior problem:

With the help of the transmission conditions $p_{S|B}^e = p_{S|B}^c$ and $\frac{\partial p_S^e}{\partial \nu^e}|_B = \frac{\partial p_S^c}{\partial \nu^c}|_B$, one gets the boundary condition for the exterior problem on $\mathcal{B}$. Let ν^e denote the unit outward normal to Ω^e, the exterior problem then reads

Find $p_S^e \in H^1(\Omega_e)/\mathbb{R}$ such that

$$\Delta p_S^e = 0 \text{ in } \Omega^e, \tag{45}$$

$$\frac{\partial p_S^e}{\partial \nu^e} = 0 \text{ on } \tilde{\Gamma}^e, \tag{46}$$

$$\frac{\partial p_S^e}{\partial \nu^e} + T_1(p_S^e) = 2\alpha \frac{A_{-1}}{R^{\alpha+1}} \cos(\alpha\theta) \text{ on } \mathcal{B}, \tag{47}$$

which can be written in a variational form

$$\left(\nabla p_S^e \,|\, \nabla q\right)_{0,\Omega^e} + \int_\mathcal{B} T_1(p_S^e) q \, d\sigma = \frac{2\alpha A_{-1}}{R^{\alpha+1}} \int_\mathcal{B} \cos(\alpha\theta) q \, d\sigma, \, \forall q \in H^1(\Omega^e)/\mathbb{R}. \tag{48}$$

$(\cdot \,|\, \cdot)_{0,\Omega^e}$ stands for the scalar product of $L^2(\Omega^e)$. Clearly, the bilinear form $(p, q) \mapsto \int_\mathcal{B} T_1(p)q \, d\sigma$ is symmetric positive. Thus, for a given A_{-1}, the above exterior problem is well-posed. In order to solve the exterior problem numerically, a triangular mesh of Ω^e is provided. The space $H^1(\Omega^e)/\mathbb{R}$ is discretized with the help of Lagrange Finite Elements: let V_h^e be the space of H^1-conforming Finite Element functions thus generated, and let p_h^e be the associated discrete solution. It can be written in the form $p_h^e = \sum_{i=1}^{N^e} p_i \lambda_i$, where $(\lambda_i)_{1 \leq i \leq N^e}$ are the basis functions of V_h^e. After the discretization, the variational formulation (48) can be written as a linear system:

$$\left(\mathbb{K}_{\Omega^e} + \mathbb{K}_\mathcal{B}\right) p_h^e = \mathbf{F}. \tag{49}$$

Here, p_h^e also stands for the vector of $\mathbb{R}^{N^e}$ of entries p_i. The matrix $\mathbb{K}_\mathcal{B}$ is "locally" full but, being defined only on the interface $\mathcal{B}$, its size remains small. For λ_i and λ_j the support of which intersects the interface, the entry $(\mathbb{K}_\mathcal{B})_{i,j}$ reads

$$\frac{2\alpha^2}{\pi R} \sum_{n \geq 1} n \left\{ \int_0^{\pi/\alpha} \lambda_i(R, \theta) \cos(n\alpha\theta) \, d\theta \int_0^{\pi/\alpha} \lambda_j(R, \theta) \cos(n\alpha\theta) \, d\theta \right\},$$

4. The computation of the coefficients A_n is carried out with the help of (40)–(42). Thus, one can reconstruct the solution in the whole domain (but not at the reentrant corner, which belongs to the boundary).

Remark 3.2. If the Maxwell equations are coupled with a particle method, such as Vlasov's equation, computing the trajectography requires that the electromagnetic field is known at every possible position of the particles, often *very close* to the boundary, but never *on* the boundary.

Second Step: Computation of $\mathbf{v}_S$

• Computation of the scalar potential: As mentioned earlier on, $\mathbf{v}_S$ is computed *via* its scalar potential ϕ_S. One solves first the system (37), (38) in a manner which is similar to the one kept for p_S.

1. The local solution ϕ_S^c reads:

$$\phi_S^c = -\sum_{n\geq 1} \frac{B_n}{n\alpha} r^{n\alpha} \cos(n\alpha\theta) - \sum_{n\geq -1} \frac{A_n}{4n\alpha + 4} r^{n\alpha+2} \cos(n\alpha\theta), \tag{50}$$

where the coefficients $(B_n)_{n\geq 1}$ can be expressed as functions of the trace ϕ_S^c on $\mathcal{B}$, that is:

$$n = 1 \quad B_1 = -\frac{2\alpha^2}{\pi R^\alpha} \int_0^{\pi/\alpha} \phi_S^c(R,\theta) \cos(\alpha\theta)\, d\theta$$
$$- \left(\frac{\alpha}{4 - 4\alpha} A_{-1} R^{2-2\alpha} + \frac{\alpha}{4 + 4\alpha} A_1 R^2 \right), \tag{51}$$

$$n \geq 2 \quad B_n = -\frac{2n\alpha^2}{\pi R^{n\alpha}} \int_0^{\pi/\alpha} \phi_S^c(R,\theta) \cos(n\alpha\theta)\, d\theta - \frac{n\alpha}{4n\alpha + 4} A_n R^2. \tag{52}$$

2. The capacitance operator t is

$$t\left(\phi_S^c\right) = T_1\left(\phi_S^c\right) - \frac{1}{2} \int_0^R p_S^c(r,\theta)\, dr + \frac{\alpha}{2 - 2\alpha} A_{-1} R^{1-\alpha} \cos(\alpha\theta). \tag{53}$$

The exterior problem, of solution ϕ_S^e, which can be written similarly to p_S^e, is equivalent to the variational formulation:
Find $\phi_S^e \in H^1(\Omega^e)/\mathbb{R}$ *such that*

$$\left(\nabla\phi_S^e \mid \nabla\psi\right)_{0,\Omega_e} + R \int_0^{\pi/\alpha} T_1\left(\phi_S^e\right)\psi(R,\theta)\, d\theta$$
$$= \left(p_S^e \mid \psi\right)_{0,\Omega_e} + \frac{1}{2} R \int_0^{\pi/\alpha} \left\{ \int_0^R p_S^c(r,\theta)\, dr \right\} \psi(R,\theta)\, d\theta$$
$$- \frac{\alpha}{2 - 2\alpha} A_{-1} R^{2-\alpha} \int_0^{\pi/\alpha} \cos(\alpha\theta)\psi(R,\theta)\, d\theta, \quad \forall\psi \in H^1(\Omega_e)/\mathbb{R}. \tag{54}$$

The solution to the exterior problem can be obtained by the Finite Element discretization of the formulation (54). Let ϕ_h^e denote the discrete solution in V_h^e, that is $\phi_h^e = \sum_{i=1}^{N^e} \phi_i \lambda_i$. It is the solution to the linear system

$$\left(\mathbb{K}_{\Omega_e} \phi_h^e + \mathbb{K}_{\mathcal{B}}\right)\phi_h^e = \mathbb{M}_{\Omega_e} p_S^e + \mathbf{G}, \tag{55}$$

where $\mathbb{M}_{\Omega_e}$ stands for the mass matrix, that is, the matrix associated to the L^2 scalar product in Ω^e. The matrix being identical to that of (49), this formulation with the potential requires only minor modifications. The coefficients B_n are then computed with the help of (51), (52), and the potential is thus known everywhere except at the reentrant corner.

- Computation of $\mathbf{v}_S$:

One simply gets $\mathbf{v}_S$ by taking the vector curl of ϕ_S.

   1. The local solution $\mathbf{v}_S^c$:

$$\mathbf{v}_S^c = \sum_{n \geq 1} B_n r^{n\alpha - 1} \begin{pmatrix} \sin(n\alpha\theta) \\ \cos(n\alpha\theta) \end{pmatrix} + \sum_{n \geq -1} A_n r^{n\alpha + 1} \begin{pmatrix} \frac{n\alpha}{4n\alpha + 4} \sin(n\alpha\theta) \\ \frac{n\alpha + 2}{4n\alpha + 4} \cos(n\alpha\theta) \end{pmatrix}, \quad \text{with } B_1 \neq 0. \tag{56}$$

   2. The exterior solution $\mathbf{v}_S^e$:

One solves the equation of unknown $\mathbf{v}_S^e$ which reads:

Find $\mathbf{v}_S^e \in (H^1(\Omega^e)/\mathbb{R})^2$ *such that*

$$\left(\mathbf{v}_S^e \mid \boldsymbol{\lambda} \right)_{0, \Omega^e} = \left(\mathbf{curl}\, \phi_S^e \mid \boldsymbol{\lambda} \right)_{0, \Omega^e}, \forall \boldsymbol{\lambda} \in (H^1(\Omega^e)/\mathbb{R})^2. \tag{57}$$

Numerically, one does not simply perform $\mathbf{v}_S = \mathbf{curl}\, \phi_S$; some straightforward interpolation is added, so that an approximation $\mathbf{v}_S^h$ is at hand. For that, the whole domain is meshed (in our case, there remains only to mesh Ω^c, in an admissible manner on $\mathcal{B}$).

Thus, in order to compute a numerical approximation of $\mathbf{v}_S$, the basis of V_S, (56) is interpolated at the vertices inside Ω^c to get $\mathbf{v}_h^c$ (the coefficients A_n and B_n have already been computed). To compute $\mathbf{v}_h^e$, (57) is discretized

$$\mathbb{M}_{\Omega^e} \mathbf{v}_h^e = \mathbb{R}_{\Omega^e} \phi_h^e, \tag{58}$$

where $\mathbb{R}_{\Omega^e}$ stands for the curl matrix, associated to the term $(\mathbf{curl}\, \phi_S^e \mid \boldsymbol{\lambda})_{0, \Omega^e}$.

Remark 3.3. The analytical solutions p_S^c, ϕ_S^c, and $\mathbf{v}_S^c$ are known *via* series (which converge, the solutions being in $L^2(\Omega^c)$), they must be *truncated* for the numerical computations. However, in practice, the series converge very rapidly (spectral convergence), which means that a small number of terms (less than 10) are sufficient to compute a solution accurately.

Remark 3.4. If, given $f \in L_0^2(\Omega)$, one wants to solve the (stationary) curl–div problem:

Find $\mathbf{u} \in H(\text{curl}, \Omega)$ *such that*

$$\text{curl } \mathbf{E} = f, \tag{59}$$

$$\text{div } \mathbf{E} = 0, \tag{60}$$

$$\mathbf{E} \cdot \boldsymbol{\tau} = 0 \text{ on } \Gamma, \tag{61}$$

one simply must split the solution of (59)–(61) as $\mathbf{E} = \mathbf{E}_R + \kappa \mathbf{v}_S$, with $\mathbf{E}_R \in V_R$, $\mathbf{v}_S$ the (known) basis of V_S and κ a constant. The orthogonality of $\mathbf{E}_R$ and $\mathbf{v}_S$ yields

$$(\text{curl } \mathbf{E} \mid \text{curl } \mathbf{v}_S)_0 = (f \mid \text{curl } \mathbf{v}_S)_0 = \kappa (\text{curl } \mathbf{v}_S \mid \text{curl } \mathbf{v}_S)_0.$$

Using (34), one finally obtains

$$\kappa = \frac{(f \mid p_S)_0}{\|p_S\|_0^2}.$$

The computation of the regular part $\mathbf{E}_R$ can then be carried out with the help of a classical numerical method. Thus, it is clear that only a few modifications are required, as long as a code, which computes the solution to similar problems in convex domains, is already at hand.

3.2. Solution to the Time-Dependent Problem

3.2.1. *The Variational Formulation*

A new variational formulation of the problem (24), (25) is introduced, using the orthogonal decomposition of $V = V_R \overset{\perp}{\oplus} V_S$, and of the solution $\mathbf{E}(t) = \mathbf{E}_R(t) + \kappa(t)\mathbf{v}_S(t)$ (cf. (30)). In an equivalent manner, we add to the space of test functions V_R the function $\mathbf{v}_S$. With this orthogonal decomposition, the classical formulation (24) can be written
Find $\mathbf{E}_R \in V_R$ such that

$$\frac{d^2}{dt^2}(\mathbf{E}_R \mid \mathbf{F}_R)_0 + c^2(\operatorname{curl}\mathbf{E}_R \mid \operatorname{curl}\mathbf{F}_R)_0$$
$$= -\frac{1}{\varepsilon_0}\frac{d}{dt}(\mathbf{J} \mid \mathbf{F}_R)_0 - \kappa''(t)(\mathbf{v}_S \mid \mathbf{F}_R)_0, \forall \mathbf{F}_R \in V_R. \tag{62}$$

This formulation projects the solution of Maxwell's equations on the space V_R of the regular fields and carries the singularity onto the space V_S. A by-product is the additional unknown $\kappa''(t)$, the second derivative of κ with respect to the time variable. Therefore, one must add an extra equation, obtained for instance by taking $\mathbf{v}_S$ as a test function.

$$\frac{d^2}{dt^2}(\mathbf{E}_R \mid \mathbf{v}_S)_0 + \kappa''(t)\|\mathbf{v}_S\|_0^2 + c^2\kappa(t)\|p_S\|_0^2 = -\frac{1}{\varepsilon_0}\frac{d}{dt}(\mathbf{J} \mid \mathbf{v}_S)_0. \tag{63}$$

Remark 3.5. In the more general case of a domain with K reentrant corners, the solution has the form (31). The space of test functions V_R is then completed with the K functions $(\mathbf{v}_S^i)_{1 \leq i \leq K}$. The formulation (24) then reads
Find $\mathbf{E}_R \in V_R$ such that

$$\frac{d^2}{dt^2}(\mathbf{E}_R \mid \mathbf{F}_R)_0 + c^2(\operatorname{curl}\mathbf{E}_R \mid \operatorname{curl}\mathbf{F}_R)_0$$
$$= -\frac{1}{\varepsilon_0}\frac{d}{dt}(\mathbf{J} \mid \mathbf{F}_R)_0 - \sum_{1 \leq j \leq K}\kappa_j''(t)(\mathbf{v}_S^j \mid \mathbf{F}_R)_0, \quad \forall \mathbf{F}_R \in V_R. \tag{64}$$

The K additional unknowns $(\kappa_j''(t))_{1 \leq j \leq K}$ appear. The above system is completed in this case with K additional equations, where the K test functions are $(\mathbf{v}_S^i)_{1 \leq i \leq K}$. Thanks to the orthogonality of regular and singular fields, one gets

$$\frac{d^2}{dt^2}(\mathbf{E}_R \mid \mathbf{v}_S^i)_0 + \sum_{1 \leq j \leq K}\kappa_j''(t)(\mathbf{v}_S^j \mid \mathbf{v}_S^i)_0 + c^2\kappa_i(t)(p_S^j \mid p_S^i)_0$$
$$= -\frac{1}{\varepsilon_0}\frac{d}{dt}(\mathbf{J} \mid \mathbf{v}_S^i)_0, 1 \leq i \leq K. \tag{65}$$

3.2.2. *Discretization of the Formulation (62), (63)*

One proceeds in two steps: first a semidiscretization in space, then a discretization in time.

Let us consider the semidiscretization in space of the variational problem (62), (63). The triangle mesh is the (admissible) union of the meshes over Ω^e and Ω^c. Let $V_R^h \subset V_R$ be the space of discretized test functions, and let $\mathbf{E}^h(t) = \mathbf{E}_R^h(t) + \kappa(t)\mathbf{v}_S$ be the discrete solution. One knows that $\mathbf{E}_R^h(t) = \sum_i E_R^i \boldsymbol{\lambda}_i$, where $\boldsymbol{\lambda}_i$ are the basis functions of the Finite Element Method. Here, $\boldsymbol{\lambda}_i$ denotes a vector basis function: one of its component is equal to λ_i, and the other is equal to zero. If it is additionaly assumed that $\mathbf{v}_S$ is known exactly, the orthogonality relationships still hold and the semidiscretized variational formulation is written (with the addition of the index $_h$) in the same way as (62), (63).

Remark 3.6. 1. The semidiscrete system derived from (62), (63) is coupled *via* the terms $\kappa''(t)$ and $\mathbf{E}_R^h(t)$. One can obtain a decoupled version with the help of the (orthogonal) projection P_h on V_R^h with respect to the scalar product of $L^2(\Omega)^2$, by taking $\mathbf{v}_S - P_h \mathbf{v}_S$ as a test function instead of $\mathbf{v}_S$. Equation (63) is then replaced by

$$\kappa''(t)\|\mathbf{v}_S - P_h\mathbf{v}_S\|_0^2 + c^2\kappa(t)\|p_S\|_0^2$$
$$= c^2\left(\operatorname{curl}\mathbf{E}_R^h \,\big|\, \operatorname{curl}(P_h\mathbf{v}_S)\right)_0 - \frac{1}{\varepsilon_0}\frac{d}{dt}(\mathbf{J}^h \,\big|\, \mathbf{v}_S - P_h\mathbf{v}_S)_0. \tag{66}$$

Actually, if one considers the linear system resulting from (62), (63), this can be viewed as the usual factorization which is performed to provide a block triangular matrix. The function κ is then computed by solving the ordinary differential equation (66). According to the regularity of $\mathbf{v}_S$ [5], the estimation of the coefficient in front of $\kappa''(t)$ yields

$$\|\mathbf{v}_S - P_h\mathbf{v}_S\|_0^2 \leq C_\varepsilon h^{2\alpha - 2\varepsilon}, \quad \forall \varepsilon > 0, \text{ where } \frac{\pi}{\alpha} \text{ is the angle at the reentrant corner.} \tag{67}$$

This allows one to conclude that this differential equation is not stiff, and so that it can be solved with a classical discretization in time. Nevertheless, the numerical experiments that we have carried out with this approach (cf. [4]) yielded results which are less precise than the one obtained using (62), (63).

2. In order to simplify the presentation, we present the case of an internal approxima-tion, that is $V_R^h \subset V_R$. This assumption is, however, not required. As a matter of fact, the formulations which we implemented in our codes are not internal. Indeed, we kept mixed formulations in which the divergence constraint is dualized (see [6]). Under these condi-tions, the discrete functions of the approximation space, called Z_R^h, are not divergence-free. One must add a Lagrange multiplier $p^h \in Q^h$ to dualize the discrete divergence condition $\operatorname{div}\mathbf{E}_R^h = 0$, where the space Q^h is chosen in such a way that the discrete inf–sup condition is satisfied. This mixed formulation consists of adding a $(p^h \,|\, \operatorname{div}\mathbf{F}_R)_0$ term to the formu-lation (62). The loss of the orthogonality between V_S and Z_R^h (as $Z_R^h \not\subset V_R$) yields another term in (62), which reads

$$\left(\operatorname{curl}\mathbf{v}_S \,\big|\, \operatorname{curl}\mathbf{F}_R^h\right)_0 \neq 0, \quad \forall \mathbf{F}_R^h \in Z_R^h. \tag{68}$$

3.2.3. Time Discretization

The formulation (62) can be written equivalently as a linear system

$$\frac{d^2}{dt^2}\mathbb{M}_\Omega \mathbf{E}_R^h + c^2 \mathbb{R}_\Omega \mathbf{E}_R^h = -\frac{1}{\varepsilon_0}\frac{d}{dt}\mathbb{M}_\Omega \mathbf{J}^h - \kappa''(t)\mathbf{\Lambda}^h, \tag{69}$$

where $\mathbb{M}_\Omega$ is the mass matrix, $\mathbb{R}_\Omega$ is the curl matrix, and $\mathbf{\Lambda}^h$ is the vector whose components are the integrals over Ω of the scalar product of $\mathbf{v}_S$ and the basis functions of V_R^h. Now, $\mathbf{v}_S$ being singular, the computation must be carried out precisely in the neighborhood of the reentrant corner. This point shall be detailed in Subsection 3.3.

Starting from (63), $\kappa''(t)$ is expressed as

$$\kappa''(t) = \frac{1}{\|\mathbf{v}_S\|_0^2}\left(-\frac{1}{\varepsilon_0}(\mathbf{J}' \mid \mathbf{v}_S)_0 - c^2\|p_S\|_0^2\kappa(t) - (\mathbf{E}_R'' \mid \mathbf{v}_S)_0\right), \tag{70}$$

where $'$ stands for the first derivative in time. This expression is included in (69). One then obtains

$$\mathbb{M}_\Omega \mathbf{E}_R'' + c^2 \mathbb{R}_\Omega \mathbf{E}_R^h = -\frac{1}{\varepsilon_0}\mathbb{M}_\Omega \mathbf{J}' + \frac{1}{\|\mathbf{v}_S\|_0^2}\left(\frac{1}{\varepsilon_0}(\mathbf{J}' \mid \mathbf{v}_S)_0 + c^2\|p_S\|_0^2\kappa(t) + (\mathbf{E}_R'' \mid \mathbf{v}_S)_0\right)\mathbf{\Lambda}^h, \tag{71}$$

which is implicit in $\mathbf{E}_R''$. After a time discretization involving a second-order explicit (leap-frog) scheme, the scheme reads

$$\mathbb{M}_\Omega \mathbf{E}_R^{n+1} - \frac{1}{\|\mathbf{v}_S\|_0^2}\left(\mathbf{E}_R^{n+1} \mid \mathbf{v}_S\right)_0 \mathbf{\Lambda}^h = \mathbf{G}^n. \tag{72}$$

The superscript ^{h} is dropped. Here the notation X^n (respectively, X^{n+1}) stands for a variable X at time $t^n = n\Delta t$ (respectively, $t^{n+1} = (n+1)\Delta t$), where Δt is the time step, and $\mathbf{G}^n = (G_x^n, G_y^n)$ is a set of quantities known at time t^n.

It can be checked in an elementary manner that the resulting linear system is invertible (cf. [4]). By construction, $\mathbf{E}_R^{n+1}$ can be decomposed over the basis functions, so that one actually has

$$\left(\mathbf{E}_R^{n+1} \mid \mathbf{v}_S\right)_0 = \sum_i \left(\Lambda_x^i \left(E_{R,x}^{n+1}\right)_i + \Lambda_y^i \left(E_{R,y}^{n+1}\right)_i\right), \tag{73}$$

where the Λ_x^i, Λ_y^i are the components of $\mathbf{\Lambda}^h$. Recall that the mass matrix $\mathbb{M}_\Omega$ is diagonalized thanks to a quadrature formula (see [6]), which preserves the accuracy. Note that this is of crucial importance, as far as the choice of the method for solving the time-dependent Maxwell equations is concerned. In this way, the linear system (72) can be written row-wise

$$m_i\left(E_{R,x}^{n+1}\right)_i - \frac{1}{\|\mathbf{v}_S\|_0^2}\sum_j \left(\Lambda_x^j\left(E_{R,x}^{n+1}\right)_j + \Lambda_y^j\left(E_{R,y}^{n+1}\right)_j\right)\Lambda_x^i = \left(G_x^n\right)_i, \tag{74}$$

$$m_i\left(E_{R,y}^{n+1}\right)_i - \frac{1}{\|\mathbf{v}_S\|_0^2}\sum_j \left(\Lambda_x^j\left(E_{R,x}^{n+1}\right)_j + \Lambda_y^j\left(E_{R,y}^{n+1}\right)_j\right)\Lambda_y^i = \left(G_y^n\right)_i, \tag{75}$$

where m_i is the ith diagonal entry of $\mathbb{M}_\Omega$. This equation can be easily solved. With obvious notations, it can be rewritten (for every i)

$$A_i X_i - \sum_j B_j X_j = F_i. \tag{76}$$

After a few algebraic manipulations, one can reach an explicit expression of the solution

$$X_i = \frac{F_i\left(1 - \sum_j \frac{B_j}{A_j}\right) + \sum_j \frac{B_j}{A_j} F_j}{A_i\left(1 - \sum_j \frac{B_j}{A_j}\right)}, \tag{77}$$

for which it is easily checked that the denominator never vanishes (cf. [4]).

Remark 3.7.   1. We presented the algorithm that allows one to compute the field at an interior node to simplify. The expression (74) is modified accordingly for a boundary node, depending on the boundary condition (absorbing boundary condition, incoming wave, symmetry, etc.), but it is always analogous to (77).

2. For similar reasons, we have not taken into account the term which stems from the dualization of the constraint on the divergence of the electric field (the reader is referred to [6] for a detailed account). In the numerical codes that we developed, this term is taken into account and the above algorithm can easily be adapted.

Once the value of $\mathbf{E}_R^{n+1}$ is computed, one can also compute, at the corresponding time, the value $\kappa^{n+1} \stackrel{\text{déf}}{=} \kappa(t^{n+1})$, with the help of a time discretization of the differential equation (70). For practical reasons, the leap-frog scheme is used again:

$$\kappa^{n+1} = 2\kappa^n - \kappa^{n-1} - c^2 \Delta t^2 \frac{\|p_S\|_0^2}{\|\mathbf{v}_S\|_0^2} \kappa^n$$
$$- \frac{\left(\mathbf{E}_R^{n+1} - 2\mathbf{E}_R^n + \mathbf{E}_R^{n-1} \mid \mathbf{v}_S\right)_0}{\|\mathbf{v}_S\|_0^2} - \frac{\Delta t}{\varepsilon_0 \|\mathbf{v}_S\|_0^2} \left(\mathbf{J}^{n+1/2} - \mathbf{J}^{n-1/2} \mid \mathbf{v}_S\right)_0. \tag{78}$$

Remark 3.8.   As far as the numerical implementation is concerned, taking into account the singularities requires only the following modifications:

1. The addition, in the classical formulation (69), of the term $\kappa''(t)\mathbf{\Lambda}^h$, and therefore the use of the modified solver (see the formula (77)),
2. The straightforward solution to the additional equation (78).

3.3. Some Details Concerning the Numerical Integration

To conclude this Section, the computation of the coefficients $\|p_S\|_0^2$ and $\|\mathbf{v}_S\|_0^2$ and the computation of the components of $\mathbf{\Lambda}^h$ are briefly presented.

1. Computation of $\|p_S\|_0^2$ and $\|\mathbf{v}_S\|_0^2$
   For the computation of $\|p_S\|_0^2$, the integral over Ω is split over $\Omega = \Omega^c \cup \Omega^e$, thus resulting in a sum of an integral over Ω^c and one over Ω^e. In Ω^c, the analytic expression (39) of p_S^c is kept. In Ω^e, the discrete form $p_h^e = \sum_i p_i \lambda_i$, with $(\lambda_i)_{1 \le i \le N^e}$, the basis

functions of V_h^e, is used. Then

$$\|p_S\|_0^2 = \int_0^R \int_0^{\frac{\pi}{\alpha}} \left(\sum_{n \geq -1} A_n r^{n\alpha} \cos(n\alpha\theta) \right)^2 r \, dr \, d\theta + \sum_{i,j=1}^{N^e} p_i \, p_j (\lambda_i \mid \lambda_j)_{0,\Omega^e}.$$

This gives

$$\|p_S\|_0^2 = \frac{\pi}{2\alpha} \left(A_{-1} A_1 R^2 + A_0^2 R^2 + \sum_{\substack{n \geq -1 \\ n \neq 0}} A_n^2 \frac{R^{2+2n\alpha}}{2 + 2n\alpha} \right) + {}^t p_h^e \mathbb{M}_{\Omega^e} \, p_h^e. \qquad (79)$$

The computation of $\|\mathbf{v}_S\|_0^2$ is carried out along the same lines.

2. Computation of $\mathbf{\Lambda}^h$.

Recall that $\mathbf{\Lambda}^h$ does not depend on the time variable, so it is computed only once. The domain is split in three subdomains Ω_i, $1 \leq i \leq 3$. One writes

$$(\mathbf{v}_S \mid \mathbf{v}_R)_0 = \sum_{i=1}^3 (\mathbf{v}_S \mid \mathbf{v}_R)_{0,\Omega_i} \qquad (80)$$

and a different numerical integration scheme is used on each subdomain, depending on the regularity of $\mathbf{v}_S$.

(a) Ω_1 is the domain which is closest to the reentrant corner: it is made up of the triangles, one of the vertices of which is the reentrant corner. It is possible, without restricting the scope of the method, to build a mesh such that Ω_1 is composed of m isoceles triangles $(T_j)_{j=1,\dots m}$, of angle $\delta\theta \overset{\text{def}}{=} \frac{\pi/\alpha}{m}$ at the reentrant corner, and with sides originating from this corner of fixed length r_1. $(\mathbf{v}_S \mid \mathbf{v}_R)_{0,\Omega_1}$ is equal to $\sum_{j=1}^m \int_{T_j} \mathbf{v}_S \cdot \mathbf{v}_{R_{1j}} d\mathbf{x}$: using the analytical expression of $\mathbf{v}_S$ (see (56)), of the basis functions $\mathbf{v}_{R_{1j}}$, and of the triangle T_j in the *polar* coordinates (r, θ), one computes the exact analytical form (in r) of $(\mathbf{v}_S, \mathbf{v}_R)_{\Omega_1}$. The only expression (in θ) which has to be numerically computed is

$$\int_0^{\frac{\delta\theta}{2}} \frac{\cos((n\alpha + k)\theta)}{\cos\theta^{(n\alpha+l)}} \, d\theta,$$

where k and l belong to $\{-1, 0, 1, 2, 3, 4\}$. It is computed with the help of a 7-point Lobatto formula, between two consecutive zeros of the integrand.

(b) Ω_2 is usually equal to $\Omega_c \backslash \Omega_1$, in which the analytical expression (56) still holds for $\mathbf{v}_S$. In the polar coordinates, the mesh being unstructured, there is not anymore an analytical expression of the basis functions. It is therefore preferable to use a numerical integration scheme (here, a 7-point Gauss formula exact up to order 5).

(c) In Ω_3 (in practice, Ω^e), $\mathbf{v}_S$ is smoother, and it has been numerically computed on the basis functions of V_h^e. In this way, $(\mathbf{v}_S \mid \mathbf{v}_R)_{0,\Omega_3}$ is computed with the same quadrature formula as the one that is used for the Finite Element basis functions.

4. THE SILVER–MÜLLER ABSORBING BOUNDARY CONDITION

Let us consider again briefly the problem set in $\Omega \times \mathbb{R}$. It is assumed here that a perfectly conducting boundary condition is applied on a part $\Gamma_C \times \mathbb{R}$ of the boundary ($\Gamma_C \subset \Gamma$) of the domain: i.e., $\mathcal{E} \times \nu = 0$ on $\Gamma_C \times \mathbb{R}$. The interaction between the domain and the exterior is modeled on the remaining part. The chosen boundary conditions are among the following: absorbing condition, incoming or outgoing waves, that is, with $\Gamma_A = \Gamma \backslash \Gamma_C$:

$$(\mathcal{E} - c\mathcal{B} \times \nu) \times \nu = \mathcal{G} \times \nu \quad \text{on } \Gamma_A \times \mathbb{R}. \tag{81}$$

In the case which is studied in this paper, that is, with the fields and the data independent on z, this condition reads in the TE mode

$$\mathbf{E} \cdot \tau - c B_z = \mathbf{g} \cdot \tau \quad \text{on } \Gamma_A. \tag{82}$$

$\mathbf{g}$ is linked to the incoming wave, which is assumed to be a smooth field, defined on Γ_A. When $\mathbf{g} = 0$, the condition (81) is actually a first-order absorbing boundary condition. It is often called the Silver–Müller condition.

Remark 4.1. Without loss of generality, it is always possible to choose the artificial boundary Γ_A in such a way that it does not touch the reentrant corner. Mathematically speaking, there exists a neighborhood $\mathcal{V}_c$ of the corner such that $\mathcal{V} \cap \Gamma_A = \emptyset$.

Let W stand for the space of solutions,

$$W = \{\mathbf{E} \in H(\text{curl}, \Omega), \text{ div } \mathbf{E} = 0, \mathbf{E} \cdot \tau = 0 \text{ on } \Gamma_C\}. \tag{83}$$

As for V, W is not included in $H^1(\Omega)^2$. Let us thus define W_R, the regularized subspace of W:

$$W_R = \{\mathbf{E} \in H^1(\Omega)^2, \text{ div } \mathbf{E} = 0, \mathbf{E} \cdot \tau = 0 \text{ on } \Gamma_C\} = W \cap H^1(\Omega)^2. \tag{84}$$

The variational formulation (21)–(23) must be modified accordingly. The integration by parts formula, which is used to obtain the formulation, produces new integral terms on Γ_A, in such a way that the new formulation reads:

Find $\mathbf{E}(t) \in H(\text{curl}, \Omega)$ such that

$$\frac{d^2}{dt^2}(\mathbf{E} \mid \mathbf{F})_0 + c\frac{d}{dt} \int_{\Gamma_A} \mathbf{E} \cdot \tau \mathbf{F} \cdot \tau \, d\sigma + c^2(\text{curl } \mathbf{E} \mid \text{curl } \mathbf{F})_0$$

$$= -\frac{1}{\varepsilon_0}\left(\frac{\partial \mathbf{J}}{\partial t} \,\middle|\, \mathbf{F}\right)_0 + c\frac{d}{dt} \int_{\Gamma_A} \mathbf{g} \cdot \tau \mathbf{F} \cdot \tau \, d\sigma \quad \forall \mathbf{F} \in H(\text{curl}, \Omega) \text{ s.t. } \mathbf{F} \cdot \tau|_{\Gamma_C} = 0, \tag{85}$$

$$\text{div } \mathbf{E} = 0 \text{ in } \Omega, \tag{86}$$

$$\mathbf{E} \cdot \tau|_{\Gamma_C} = 0. \tag{87}$$

4.1. A Decomposition of the Solution in Regular and Singular Parts

The singular behavior of the solution comes from the shape of the domain. Thus, it is interesting to keep the same space V_S of singular solutions ($V_S \subset W$). Indeed, one can prove that (see [4]) W can be decomposed into

$$W = W_R \oplus V_S, \tag{88}$$

where W_R is the subspace of regular solutions (84). In this case, the decomposition is not orthogonal. However, we choose to use it instead of an orthogonal decomposition, as it allows one to keep $\mathbf{v}_S$ (the basis function of V_S) as a test function. The advantage of $\mathbf{v}_S$ is that it does not depend on the time variable t, and therefore it is computed once and for all (see the remark below).

Remark 4.2. 1. The loss of orthogonality has almost no consequences as far as the numerical computations are concerned. It yields two additional terms in the final formulation (see the details hereafter).

2. One can also split further W_R in $W_R = V_R \oplus V_A$, with V_R defined by (20) (then $\mathbf{v}_R \in V_R$ is such that $\mathbf{v}_R \cdot \tau|_\Gamma = 0$). The subspace V_A can be characterized as the set of solutions of the problem

$$\operatorname{curl} \mathbf{v}_A = \operatorname{curl}(\mathbf{w}_R - \mathbf{v}_R) \text{ in } \Omega, \tag{89}$$

$$\operatorname{div} \mathbf{v}_A = 0 \text{ in } \Omega, \tag{90}$$

$$\mathbf{v}_A \cdot \tau = 0 \text{ in } \Gamma_C, \tag{91}$$

$$\mathbf{v}_A \cdot \tau = c B_z(t) + \mathbf{g}(t) \cdot \tau \text{ on } \Gamma_A. \tag{92}$$

With this decomposition, the nonvanishing term $(\operatorname{curl} \mathbf{w}_R \mid \operatorname{curl} \mathbf{v}_S)_0$, for $\mathbf{w}_R \in W_R$ and $\mathbf{v}_S \in V_S$, is reduced to $(\operatorname{curl} \mathbf{v}_A \mid \operatorname{curl} \mathbf{v}_S)_0$. This can be viewed as a "weak" orthogonality property between W_R in V_S. The drawback of this method is that it requires the computation of $\mathbf{v}_A$ at each discrete time, thus increasing the overall cost of the method by a large factor.

3. In a similar manner, one could write an orthogonal decomposition of W of the form $W = W_R \overset{\perp}{\oplus} W_S$, where W_S is the finite dimensional space of singular solutions, which satisfies the Silver–Müller boundary condition. Unfortunately, this condition is time-dependent: the subspace W_S is also be time-dependent, and the use of this second orthogonal decomposition would again require the computation of a basis function at each discrete time.

With the decomposition (88), if we let $\mathbf{E}_R(t)$ be the regular part of the solution which belongs to W_R, a formulation analogous to (62) can be written,
Find $\mathbf{E}_R \in W_R$ such that

$$\frac{d^2}{dt^2}(\mathbf{E}_R \mid \mathbf{F}_R)_0 + c \frac{d}{dt} \int_{\Gamma_A} \mathbf{E}_R \cdot \tau \, \mathbf{F}_R \cdot \tau \, d\sigma + c^2 (\operatorname{curl} \mathbf{E}_R \mid \operatorname{curl} \mathbf{F}_R)_0 + c^2 \kappa(t)(p_S \mid \operatorname{curl} \mathbf{F}_R)_0$$

$$= -\frac{1}{\varepsilon_0} \frac{d}{dt}(\mathbf{J} \mid \mathbf{F}_R)_0 + c \frac{d}{dt} \int_{\Gamma_A} \mathbf{g} \cdot \tau \mathbf{F}_R \cdot \tau \, d\sigma - \kappa''(t)(\mathbf{v}_S \mid \mathbf{F}_R)_0, \quad \forall \mathbf{F}_R \in W_R, \tag{93}$$

where the only additional term (generated by the loss of orthogonality) is $c^2 \kappa(t)(p_S \mid \operatorname{curl} \mathbf{F}_R)_0$.

An equation is added in order to compute $\kappa(t)$, with $\mathbf{v}_S$ as a test function:

$$\frac{d^2}{dt^2}(\mathbf{E}_R \mid \mathbf{v}_S)_0 + \kappa''(t)\|\mathbf{v}_S\|_0^2 + c^2(\operatorname{curl} \mathbf{E}_R \mid p_S)_0 + c^2 \kappa(t)\|p_S\|_0^2 = -\frac{1}{\varepsilon_0} \frac{d}{dt}(\mathbf{J} \mid \mathbf{v}_S)_0. \tag{94}$$

The additional term is $c^2(\operatorname{curl} \mathbf{E}_R \mid p_S)_0$. It is worth mentioning that there is no integral over Γ_A in (94), as $\mathbf{v}_S \cdot \tau|_{\Gamma_A} = 0$. This can be viewed as another advantage of the chosen formulation.

There remains to semidiscretize the formulation (93), (94) in space, which is done in a way similar to the one of the perfectly conducting boundary case. It is enough to take into

account the two additional terms already mentioned (see above), which must be computed accurately in the neighborhood of the reentrant corner (NB. The integrals over Γ_A are computed classicaly, since $\mathcal{V}_c \cap \Gamma_A = \emptyset$). To carry out those computations, the starting point is the evaluation of

$$(p_S \mid \operatorname{curl} \boldsymbol{\lambda}_i)_0, \tag{95}$$

where $(\boldsymbol{\lambda}_i)_i$ is the set of basis functions of the Finite Element Method. These terms are computed in the same manner that is proposed for the components of Λ_h (see Section 3.3): Ω is partitioned in three subdomains $(\Omega_i)_{1 \le i \le 3}$, and a different numerical integration scheme is kept on each of them, depending upon the regularity of p_S.

- In the innermost subdomain Ω_1 (the first ring of triangles surrounding the corner), $(\boldsymbol{\lambda}_i)_i$ and $p_S|_{\Omega_1} = p_S^c$ are known exactly (in polar coordinates): (95) is computed analytically.
- In the subdomain Ω_2 (equal to $\Omega^c \backslash \Omega_1$), the mesh is unstructured, so that no expression of $(\boldsymbol{\lambda}_i)_i$ is available in polar coordinates, whereas $p_S = p_S^c$ is still known analytically. An integration scheme exact up to the order 5 is chosen.
- In the exterior subdomain Ω_3 (in practice Ω^e), p_S is smooth, and it has been numerically determined as a linear combination of the basis functions of V_h^e. Equation (95) is then obtained thanks to the same scheme that has already been used for the smooth functions.

After a discretization in time *via* an explicit scheme, one must check that the two additional terms are available at the previous discrete time in order to compute $\mathbf{E}_R^{n+1}$. In this way, the scheme can be rewritten in a form similar to (74), and the same algorithm can therefore be used, with the boundary condition taken into account (see [4] for the details of implementation).

5. NUMERICAL RESULTS

The set of cases encompassed within our presentation allows one to evaluate the code-related performances of the *Singular Complement Method (SCM)*. It has been checked that the additional memory requirements are negligible. Moreover, the time needed to compute the basis of V_S during the initialization step and the solution to the supplementary equation at each discrete time is very small. About the presentation of the numerical results, we have chosen to compare them to analytical results (whenever available), or to results computed by other codes.

5.1. Computation of a Basis of V_S and Comparison to Analytical Solutions

First, let us evaluate the precision of the SCM by building a test case for which the analytical expressions of p_s^a, ϕ_S^a, and $\mathbf{v}_S^a$ are known. For that, let us consider the domain Ω made up of three quarters of a disc, centered at the origin, of radius R_e, thus presenting a reentrant corner with angle $\pi/\alpha = 3\pi/2$. The mesh is represented of Fig. 4. Note that the results below remain true for all values of $\alpha \in]1/2, 1[$.

Remark 5.1. The domain Ω is not a polygon. However, the results of the previous Sections are still valid, since Ω is locally convex at all the other corners of the boundary and, anyhow, the mesh is a polygonal approximation of Ω.
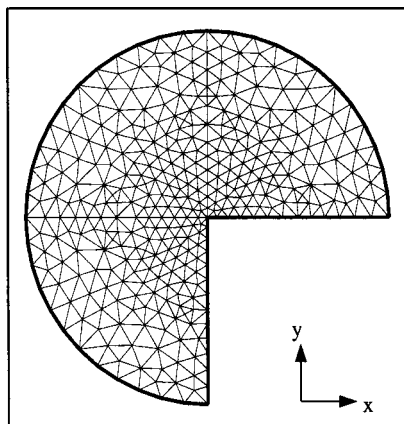
FIG. 4. The mesh.

In order to find the analytical solution to problem (32), (33), it is better to use the polar coordinates (r, θ) centered at the origin, and to look for a solution of the form

$$p_S^a(r, \theta) = \sum_{n \geq -1} A_n r^{n\alpha} \cos(n\alpha\theta) \tag{96}$$

with an arbitrary nonzero A_{-1}. A_0 is the mean value of p_S over Ω: $p_S \in L_0^2(\Omega)$ yields $A_0 = 0$. A_1 is determined with the help of the condition $\partial p_S^a / \partial v = 0$ on the boundary $r = R_e$ (but not directly from (41)), so that $A_1 = A_{-1} R_e^{-2\alpha}$. Now,

$$A_{-1} \left(r^{-\alpha} + R_e^{-2\alpha} r^\alpha \right) \cos(\alpha\theta)$$

satisfies (32), (33). The uniqueness of the solution then leads to the conclusion that $A_n = 0$, for all $n \geq 2$.

In the same way, one can look for the solution ϕ_S^a of the problem (37), (38) of the form (50), that is

$$\phi_S^a = -\sum_{n \geq 1} \frac{B_n}{n\alpha} r^{n\alpha} \cos(n\alpha\theta) - A_{-1} \left(\frac{1}{4 - 4\alpha} r^{2-\alpha} + \frac{R_e^{-2\alpha}}{4 + 4\alpha} r^{2+\alpha} \right) \cos(\alpha\theta),$$

and compute B_1 so that the boundary condition $\partial \phi_S^a / \partial v (R_e, \theta) = 0$ is satisfied (for $\theta \in]0, 3\pi/\alpha[$). Thus,

$$B_1 = A_{-1} \frac{\alpha^2 - 2}{2\alpha^2 - 2} R_e^{2-2\alpha}.$$

As before, thanks to the uniqueness of the solution $B_n = 0$ for all $n \geq 2$.

Now, with $(A_n)_n$ and $(B_n)_n$ thus determined, it is a simple matter to check that the expression of $\mathbf{v}_S^c$ given by (56) is the analytical solution $\mathbf{v}_S^a$.
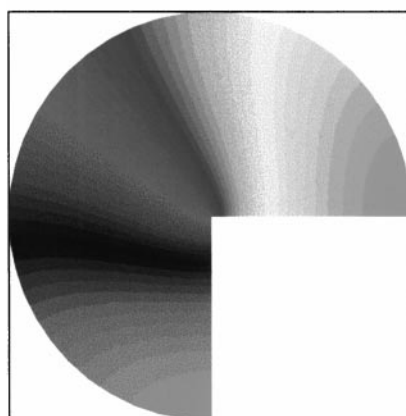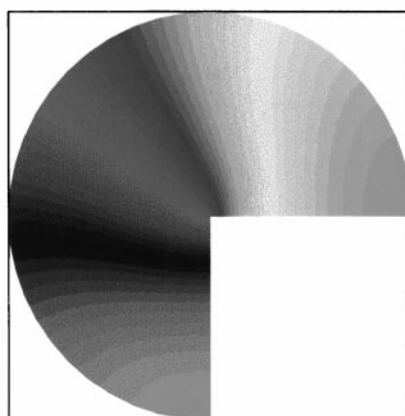
The analytical and computed solutions are pictured in Fig. 5 (with identical scales). When representing functions or fields with a singular behavior, instead of truncating the results, we have chosen to exclude the (infinite) singular node value, so as not to "flatten" the image by an arbitrary truncation value.
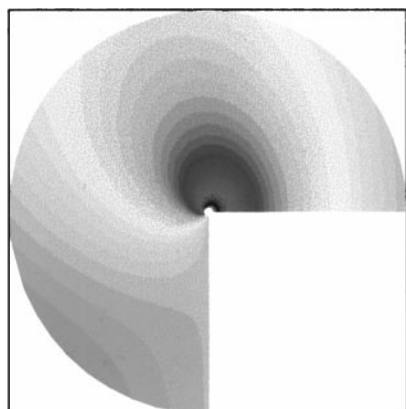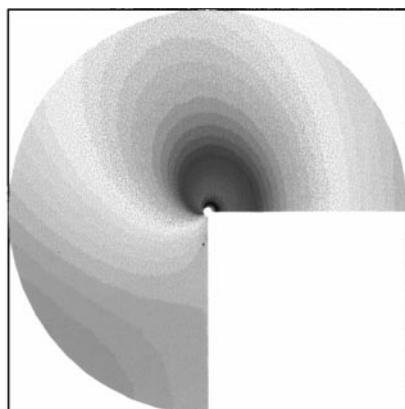
analytical v_s^y 5a v_s^y computed with the singular complement method
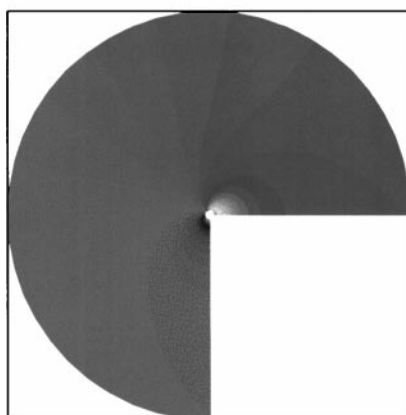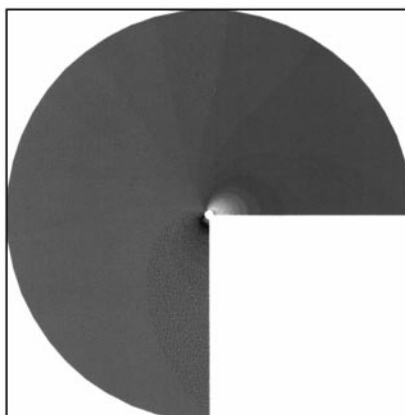
analytical p_s 5b p_s computed with the singular complement method

analytical ϕ_s 5c ϕ_s computed with the singular complement method

FIG. 5. Analytical solutions and computed solutions.

In Fig. 5a, one can see that the SCM captures well the field $\mathbf{v}_S \in V_S$ near the corner (and far away from it). Again, a conforming P^1 Finite Element Method cannot yield such a result. In addition, the quantitative results are in very good accordance, even though the mesh is not particularly refined near the corner. In Fig. 5b, one can check that the method is also efficient to compute the most singular term. This behavior is not so obvious to capture with an edge Finite Element (conforming in $H(\text{curl})$). Finally, the result on the smooth function ϕ_S (see Fig. 5c), $\phi_S \in H^{1+\alpha-\epsilon}$, $\forall \epsilon > 0$, shows that the method is efficient for more regular functions or fields: it generalizes the singular function method.

5.2. Time-Dependent Cases

In this section, the quality of the SCM is evaluated numerically on three cases. Those three cases are representative of situations that occur frequently when one is dealing with the interactions of particles and electromagnetic fields.

For instance, on the study of klystrons, one must consider the effect of a cavity on an electron beam. Thus, the first case focuses on the evolution in time of a cavity mode in a cavity with a geometrical singularity. In the second instance, one computes the electromagnetic field generated by a current, the space and time characteristics of which are similar to those of a bunched beam of particles. Then, commonly studied devices such as hyperfrequency systems often include waveguides, either to conduct the field that excites the particles, or to conduct the field induced by them. So, in the last example, a guided wave which propagates in a standard geometry is investigated.

Note that in order to evaluate the performances of our code properly, simplified examples are presented, which are still representative of the difficulties one is usually faced with (for more involved simulations, see [4]).

5.2.1. The Evolution in Time of a 2D Cavity Mode

In this first case, the study of the numerical response of a cavity excited by one of its eigenmodes is presented. The same geometry and the same mesh as in the previous example are used, once again to measure the quality of the numerical solution. To compute the analytical solution, one considers the domain Ω of Fig. 4, and Maxwell's equations (1)–(4) with $\mathbf{J} = 0$ and $\rho = 0$, written in the form of a vector wave equation. One then looks for a solution of the type

$$\mathbf{E}(\mathbf{x}, t) = \mathbf{E}(\mathbf{x}) \exp(\iota \omega t), \tag{97}$$

so that $\mathbf{E}(\mathbf{x})$ satisfies to a Helmholtz vector problem (with $k = \frac{\omega}{c}$ the wave number)

$$\mathbf{curl}\,\text{curl}\,\mathbf{E} - k^2 \mathbf{E} = 0 \text{ in } \Omega, \tag{98}$$

$$\text{div}\,\mathbf{E} = 0 \text{ in } \Omega, \tag{99}$$

$$\mathbf{E} \cdot \tau = 0 \text{ on } \Gamma. \tag{100}$$

As before, one looks for a solution using the polar coordinates (r, θ). More precisely, with the help of an *a priori* separation of variables, one finds that the

field

$$\mathbf{E}(r, \theta) = \begin{pmatrix} E_r \\ E_\theta \end{pmatrix} = \begin{pmatrix} \sum_{n \geq 1} C_n r^{-1} J_{n\alpha}(kr) \sin(n\alpha\theta) \\ \sum_{n \geq 1} C_n \frac{1}{n\alpha} \frac{d}{dr} J_{n\alpha}(kr) \cos(n\alpha\theta) \end{pmatrix}, \tag{101}$$

is a local solution of the problem, where $(C_n)_n$ are constants and $(J_{n\alpha}(\cdot))_n$ are Bessel functions (N.B. the index of a Bessel function can be any real number). The series starts at $n = 1$ in order to keep only terms which belong to $H(\mathrm{curl}, \Omega) \cap H(\mathrm{div}, \Omega)$. In addition to the local properties (98), (99), the solution must also satisfy the boundary condition (100) on the boundary $r = R_e$, so one gets

$$\frac{d}{dr} J_{n\alpha}(kR_e) = 0. \tag{102}$$

Solving the Eq. (102) amounts to finding k so that kR_e be a zero of the first derivative of the Bessel function $J_{n\alpha}$. The index $n\alpha$ being real, there exists an infinite number of zeros, every one of them being simple (to the possible exception of $kR_e = 0$, but this is excluded in the present situation as one would find that the related eigenmode vanishes). Let $j'_{n\alpha,s}$ denote the sth nonnegative zero of $J'_{n\alpha}$. In this instance, the following values are chosen: $C_1 = 1$ and $C_n = 0$, for $n \geq 2$; in this way, the solution belongs to $H(\mathrm{curl}, \Omega) \cap H(\mathrm{div}, \Omega)$, *but not to* $H^1(\Omega)^2$. $j'_{\alpha,1} = k_1 R_e$ is numerically computed, and we have $j'_{\alpha,1} \simeq 1.401$. The associated frequency is denoted by $\omega_1 = \frac{j'_{\alpha,1}c}{R_e}$.

For the time-dependent case, i.e., (97) with $\omega = \omega_1$, the initial conditions at time $t = 0$ are given by the analytical solution derived above. Figure 6 depicts the component E_x of the computed solution after 2500 time steps and the analytical solution at the same time (after 4.25 periods). One can see that the SCM yields a very accurate computation, without any mesh refinement. It should be noted that the CPU time required for such a computation is on the order of a few seconds on a common workstation.

To provide a different point of view, we also present in Fig. 7 the solutions at a given location as a function of time, with the SCM or without it. It is worth mentioning that, without the SCM, neither the frequency nor the amplitude are captured: the solution which is computed in this case *is not equal to* the solution of the Eqs. (97)–(100).
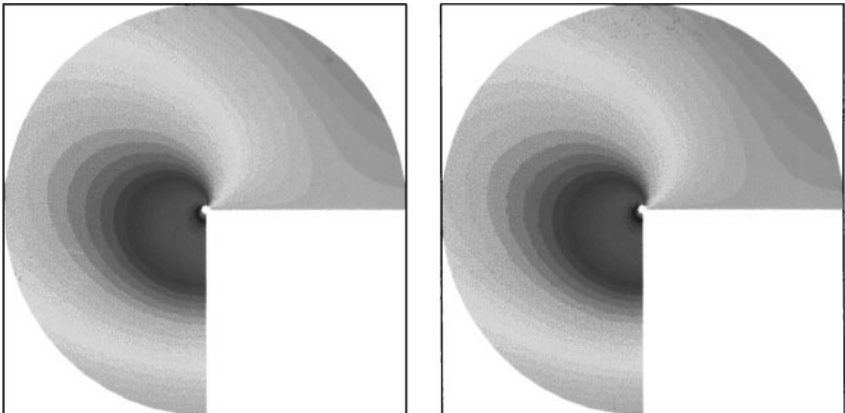

FIG. 6. Isovalues of E_x, analytical (left) and computed (right) after 4.25 periods.
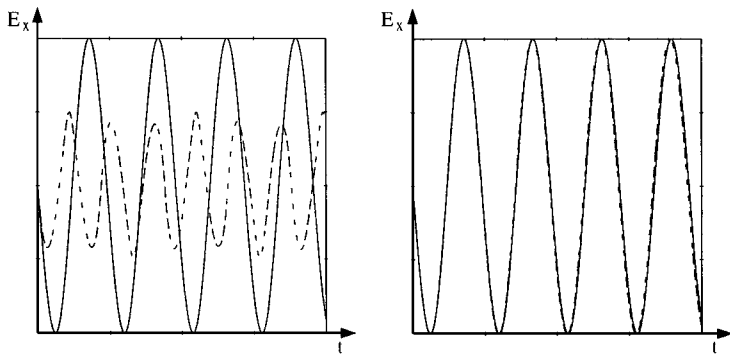
FIG. 7. Component E_x at a given location as a function of time, without the SCM (left) and with the SCM (right). The analytical solution is represented by a line, and the computed solutions are represented by a dotted line.

Let us conclude the study of the first case by examining the behavior of the code when it must capture a smooth solution. Indeed, as mentioned earlier, the regularity in space of the solution $\mathbf{E}(\mathbf{x}, t)$ (in particular any eigenmode), does not depend only on the geometry, but also on the regularity of the initial data. In this way, for an initial data of the form (101) with $C_1 = 0$, the solution is H^1 in space for all time t, and as a consequence it does require *a priori* no specific treatment such as the SCM. We checked that, in this case, the code with the SCM still computes the solution well. For that, let us chose the coefficients $C_1 = 0$, $C_n = 0$, for $n \geq 3$, and $C_2 \neq 0$, and the corresponding $j'_{\alpha,2}$. The values (see Fig. 8), computed and analytical, are very close to one another. Also, one gets that the values of κ^n all vanish (cf. Remark 2.2). There are no artificially generated singularities.

5.2.2. *Example with a Current J*

In this second instance, an L-shaped domain Ω is considered, see Fig. 9. A perfectly conducting boundary condition is imposed. The initial conditions are set to zero. The electromagnetic wave is generated by a current $\mathbf{J}(\mathbf{x}, t) = (J_x, J_y)$, the support of which is presented in the same figure, with $(J_x, J_y) = (0, 10 \sin(\omega t))$, for ω associated to a frequency of 2.5×10^9 Hertz.
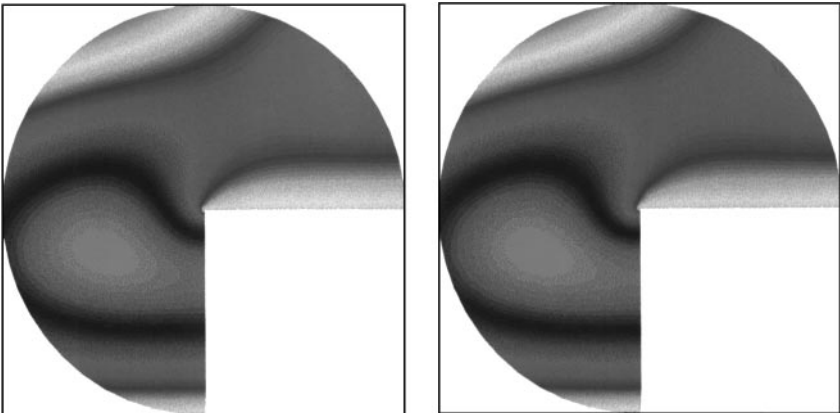

FIG. 8. Isovalues of E_x, analytical (left) and computed (right) for a smooth eigenmode.
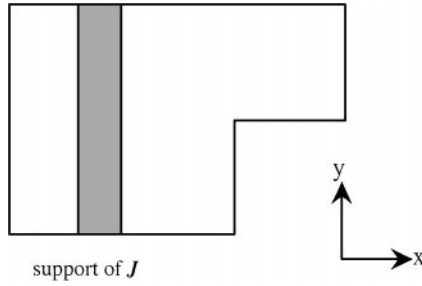
FIG. 9.   L-shaped domain and support of the current.

This current generates a wave which propagates both on the left and on the right. Physically, as long as the wave has not reached the reentrant corner, the field is smooth. Let t_s be the impact time, then, if one writes

$$\mathbf{E}(\mathbf{x}, t) = \mathbf{E}_R(\mathbf{x}, t) + \kappa(t)\mathbf{v}_S(\mathbf{x}),$$

$\kappa(t)$ is equal to zero for all t lower than t_s, and so $\mathbf{E}_R(\mathbf{x}, t)$ and $\mathbf{E}(\mathbf{x}, t)$ coincide. Now, on the one hand, for t greater than t_s, $\kappa(t) \neq 0$, and the support of $\mathbf{v}_S$ being nonlocal (in fact, the support of $\mathbf{v}_S$ spans the whole of Ω), one has $\kappa(t)\mathbf{v}_S(\mathbf{x}) \neq 0$, for all $\mathbf{x} \in \Omega$ and $t > t_s$. On the other hand, however, one wishes to reproduce the obvious physical behavior, which is that for any point $\mathbf{x}$ and time t, $\mathbf{E}(\mathbf{x}, t) = 0$ if $t < t_{\mathbf{x}}$, where $t_{\mathbf{x}}$ denotes the time at which the wave reaches $\mathbf{x}$.

One can check (see Fig. 10) that $\mathbf{E}_R(\mathbf{x}, t)$ takes nonzero values, and therefore that it "compensates" for $\kappa(t)\mathbf{v}_S(\mathbf{x})$, i.e., $\mathbf{E}_R(\mathbf{x}, t) = -\kappa(t)\mathbf{v}_S(\mathbf{x})$. Thus, $\mathbf{E}(\mathbf{x}, t)$ remains equal to zero while $t_s < t < t_{\mathbf{x}}$.

In this instance, it is not possible to provide an analytical solution. Instead, let us compare our results to the computations made by another code, based on *Finite Volume (FV)* techniques *à la* Delaunay-Voronoi [18].
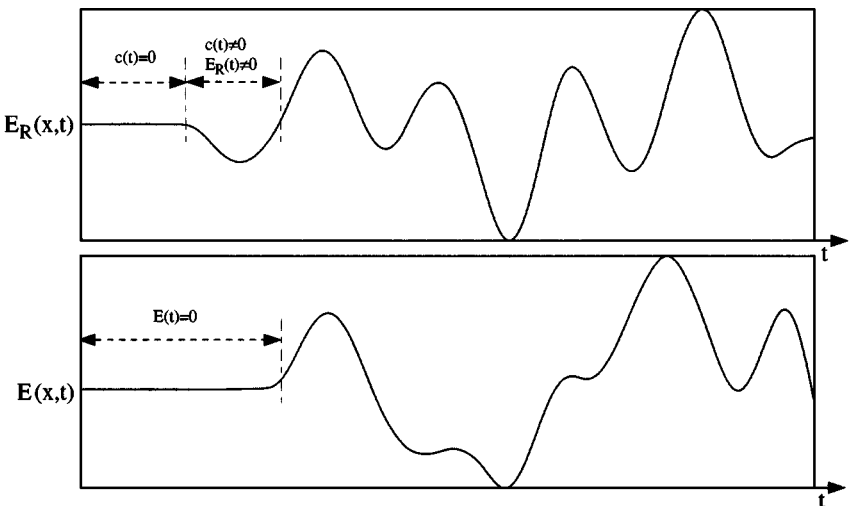

FIG. 10.   At a given point $\mathbf{x}_0$, comparison of $\mathbf{E}_R(\mathbf{x}_0, t)$ (top) and $\mathbf{E}(\mathbf{x}_0, t)$ (bottom) with t varying.
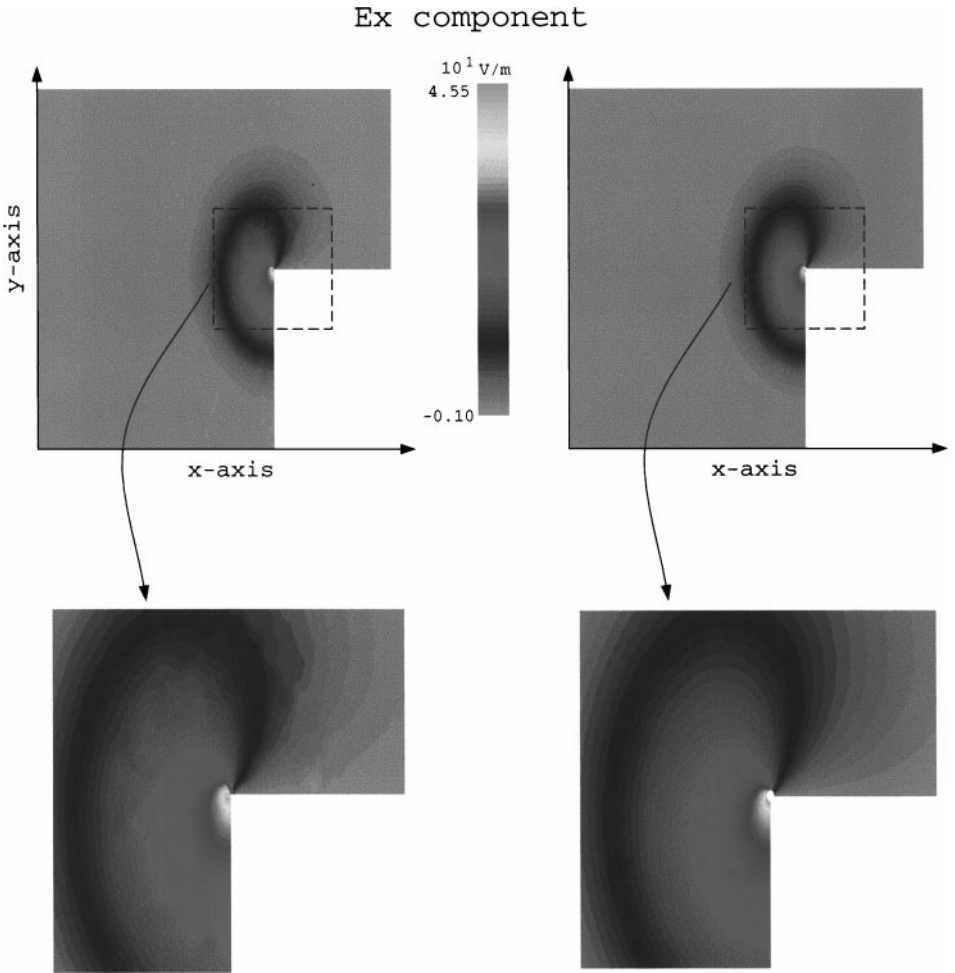
FIG. 11.   Component E_x, computed by FV (left) and by the SCM (right).

As mentioned in the Introduction, this method allows one to approximate the solution in a neighborhood of the reentrant corner (with an appropriate mesh refinement), the degrees of freedom being located on the edges. Figure 11 shows the isovalues of the electric field (after 500 time steps), which has been computed by the two methods on the same mesh. The SCM yields a better precision near the corner, as the form of the singular part is explicitly taken into account. For the SCM, the maximum value (corner excepted) is 10% higher, and the overall behavior is less noisy. Finally, the results obtained by both methods on the smooth (cf. [1]) component B_z of the magnetic induction are almost identical. This emphasizes once more that the difference stems from the singular part.

5.2.3. *The Waveguide Case*

In this last example, the propagation of a TE wave in a singular geometry is studied numerically. This case provides an interesting illustration of the possibilities of the method, when it is used on a more "complete" formulation, that is, with different types of boundary conditions. A step waveguide is considered, for which the geometry and the data do
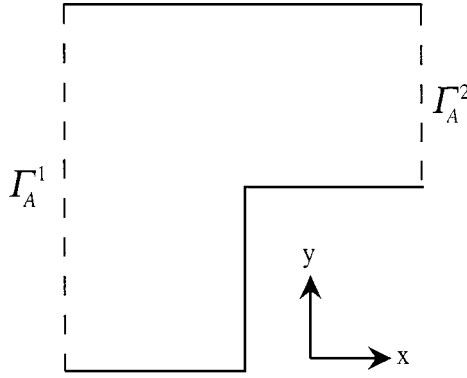
FIG. 12. Geometry of the waveguide.

not depend on the variable z. As noticed earlier, the computational domain reduces to a transversal section, pictured in Fig. 12. An incident wave enters the waveguide through the boundary Γ_A^1, and exists through Γ_A^2. This behavior is modeled thanks to the boundary condition (81), which is expressed as

$$\mathbf{E} \cdot \tau - c B_z = g, \quad g(t)|_{\Gamma_A^1} = C \sin(\omega t), \quad g(t)|_{\Gamma_A^2} = 0, \tag{103}$$

where C is a constant and ω is associated to the frequency 2.5×10^9 Hertz. At the initial time $t = 0$, the electromagnetic field is equal to zero all over the guide. As in the preceding case, the field is smooth until the wave reaches the reentrant corner, and then it becomes singular.

The result obtained *via* the classical nodal FE code (without the SCM) is presented in Fig. 13, and it shows a most unlikely approximation of the true solution (no singular behavior).

As usual, the same computation with the addition of the SCM has been carried out, and the result has been compared to that produced by the FV code. Figure 14 depicts the isovalues of the first component of the electric field after 1000 time steps.
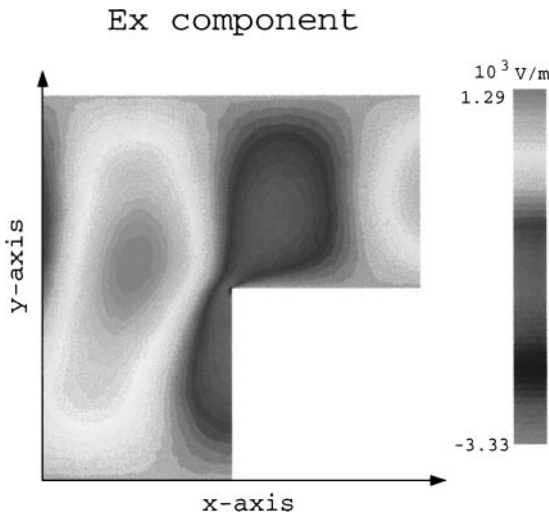
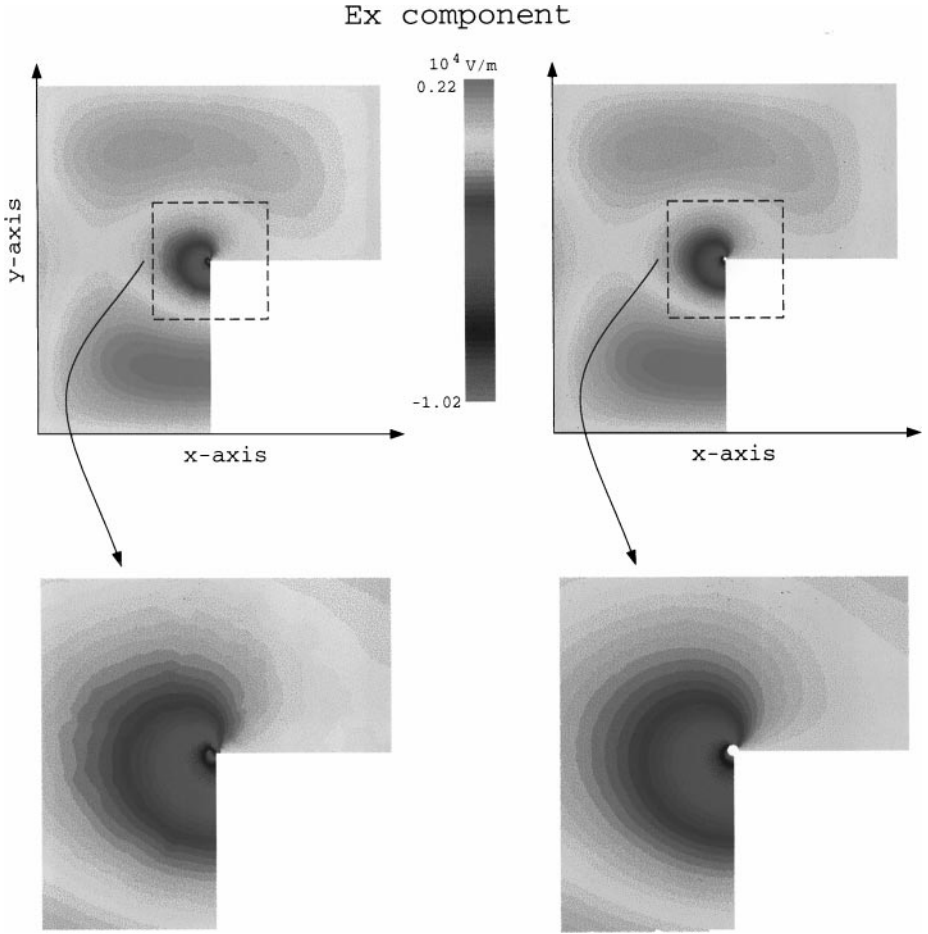**FIG. 13.** Isovalues of E_x, without the SCM.

FIG. 14. Component E_x, computed by FV (left) and by the SCM (right).

Once again, the SCM provides a numerical solution which is globally less noisy, and more precise in the neighborhood of the corner (for the SCM, the maximum value (corner excepted) is 10% higher). Finally, the results are almost identical for B_z.

6. CONCLUSION AND PERSPECTIVES

In this paper, we presented a method which allows one to solve (theoretically and) numerically Maxwell's equations in nonsmooth and nonconvex domains, the so-called *Singular Complement Method*. It is built from the mathematical analysis of the singularities generated by the geometry in Maxwell's equations. We further inferred a numerical algorithm, which can be easily included into already existing nodal FE codes.

In 2D, the mathematical analysis has been carried out, a numerical scheme has been proposed and implemented, and the code is operational. Numerical simulations have shown its efficiency in a series of examples based on practical devices. We presented a few elementary, but significant, examples of concrete situations one is faced with when handling particle–field interaction problems. For instance, we checked that the SCM allows one to simulate cavity fields, the governing phenomenon of klystron-like devices. In the same

way, we computed the propagation of electromagnetic waves in waveguides with nons-mooth boundaries thanks to the SCM. This shows that it can be used to realize an extensive study of stub filters. In addition, it can be coupled to particle methods (cf. [2]).

Handling 3D-axisymmetric domains is also possible [3], and numerical experiments are under way. The main theoretical aspects of the generalization to general 3D domains are now analyzed and well understood. Currently, we devote our attention to the development of an efficient numerical algorithm to handle the singularities in 3D.

REFERENCES

1. F. Assous and P. Ciarlet, Jr., Quelques résultats sur la régularité en temps des équations de Maxwell instation-naires, *C. R. Acad. Sci. Paris* **327**, Série I, 719 (1998).

2. F. Assous, P. Ciarlet, Jr., and E. Garcia, Résolution des équations de Maxwell instationnaires avec charges dans un domaine singulier bidimensionnel, *C. R. Acad. Sci. Paris* **330**, Série I, 391 (2000).

3. F. Assous, P. Ciarlet, Jr., and S. Labrunie, Caractérisation de la partie singuliére et résolution des équations de Maxwell en géométrie singuliére axisymétrique, *C. R. Acad. Sci. Paris* **328**, Série I, 767 (1999).

4. F. Assous, P. Ciarlet, Jr., and J. Segré, Résolution des équations de Maxwell dans un domaine 2D avec coins rentrants: Expériences numériques, in preparation.

5. F. Assous, P. Ciarlet, Jr., and E. Sonnendrücker, Resolution of the Maxwell equations in a domain with reentrant corners, *Modél. Math. Anal. Numér.* **32**, 359 (1998).

6. F. Assous, P. Degond, E. Heintzé, P. A. Raviart, and J. Segré, On a finite element method for solving the three-dimensional Maxwell equations, *J. Comput. Phys.* **109**, 222 (1993).

7. C. K. Birdsall and A. B. Langdon, *Plasmas Physics via Computer Simulation* (Mc Graw-Hill, New York, 1985).

8. A.-S. Bonnet-Ben Dhia, C. Hazard, and S. Lohrengel, A singular field method for the solution of Maxwell's equations in polyhedral domains, *SIAM J. Appl. Math.* **59**, 2028 (1999).

9. P. Ciarlet, Jr., and J. Zou, Fully discrete finite element approaches for time-dependent Maxwell's equations, *Numer. Math* **82**, 193 (1999).

10. M. Dauge, *Elliptic Boundary Value Problems on Corner Domains*, Lecture Notes in Mathematics, Vol. 1341 (Springer Verlag, Berlin, 1988).

11. R. Dautray and J. L. Lions, *Analyse mathématique et calcul numérique pour les sciences et les techniques*, 5 (Masson, Paris, 1988–1990).

12. G. J. Fix, S. Gulati, and G. I. Wakoff, On the use of singular functions with finite element approximations, *J. Comput. Phys.* **13**, 209 (1976).

13. D. Givoli, L. Rivkin, and J. B. Keller, A finite element method for domains with corners, *Int. J. Num. Meth. Eng.* **35**, 1329 (1992).

14. P. Grisvard, Elliptic problems in nonsmooth domains, in *Monographs and Studies in Mathematics*, Vol. 24 (Pitman, London, 1985).

15. P. Grisvard, *Singularities in Boundary Value Problems*, RMA 22 (Masson, Paris, 1992).

16. C. Hazard and M. Lenoir, On the solution of time-harmonic scattering problems for Maxwell's equations, *SIAM J. Math. Anal.* **27**, 1597 (1996).

17. C. Hazard and S. Lohrengel, A singular field method for Maxwell's equations: Numerical aspects in two dimensions, *SIAM J. Appl. Math.*, submitted.

18. F. Hermeline, Two coupled particle-finite volume methods using Delaunay-Voronoi meshes for the approxi-mation of Vlasov–Poisson and Vlasov–Maxwell equations, *J. Comput. Phys.* **106**, 1 (1993).

19. J. B. Keller and D. Givoli, An exact non-reflecting boundary condition, *J. Comp. Phys.* **82**, 172 (1988).

20. J. -L. Lions and E. Magenes, *Problèmes aux limites non homogènes et applications* (Dunod, Paris, 1968).

21. J. C. Nédélec, Mixed finite elements in $\mathbb{R}^3$, *Numer. Math.* **35**, 315 (1980).

22. J. C. Nédélec, A new family of mixed finite elements in $\mathbb{R}^3$, *Numer. Math.* **50**, 57 (1986).